Received: 27 January 2019 | Revised: 19 March 2019 | Accepted: 19 March 2019

DOI: 10.1002/aoc.4943

FULL PAPER

WILEY Applied Organometallic Chemistry

Fabrication, spectroscopic characterization, calf thymus DNA binding investigation, antioxidant and anticancer activities of some antibiotic azomethine Cu(II), Pd(II), Zn(II) and Cr(III) complexes

Ahmed M. Abu-Dief[1] | Hussein M. El-Sagher[1] | Mohamed R. Shehata[2]

[1]Chemistry Department, Faculty of Science, Sohag University, 82524, Egypt

[2]Chemistry Department, Faculty of Science, Cairo University, Giza, Egypt

Correspondence
Ahmed M. Abu-Dief, Chemistry Department, Faculty of Science, Sohag University, 82524, Egypt.
Email: ahmed_benzoic@yahoo.com

This study was conducted to prepare novel azomethine chelates of Cu(II), Pd(II), Zn(II) and Cr(III) with tridentate dianionic azomethine OVAP ligand 2-[(2-hydroxyphenylimino)methyl]-6-methoxyphenol. The prepared compounds were characterized using elemental analyses and spectral, conductivity, magnetic and thermal measurements. The spectroscopic data suggest that the parent azomethine ligand binds to the investigated metal ions through both deprotonated phenol oxygen and azomethine nitrogen atoms, and adopts distorted octahedral geometry in the case of Cr(III) and Cu(II) ions while tetrahedral and square planar geometries for Zn(II) and Pd(II) ions, respectively. In order to confirm the molecular geometry of the investigated azomethine chelator and its complexes, theoretical density functional theory calculations were employed. Correlation between experimental observations and theoretical calculations of geometry optimization results are in a good agreement. Absorption titration was used to explore the interaction of the investigated azomethine metal chelates with calf thymus DNA, and the binding constant as well as Gibbs free energy were evaluated. Viscosity measurements and gel electrophoresis studies suggest intercalative and replacement binding modes of the azomethine metal chelates with calf thymus DNA. Additionally, the antimicrobial activity of the complexes was screened against some pathogenic bacteria and fungi. This biological study shows that the complexes exhibit a marked inhibitory effect compared to the corresponding ligand and standard drug**s.** Furthermore, the effect of the novel compounds as antioxidants was determined by reduction of 1,1-diphenyl-2-picrylhydrazyl and compared with that of vitamin C. Finally, *in vitro* cell proliferation via MTT assay was investigated against colon carcinoma cells (HCT-116), hepatic cellular carcinoma cells (HepG-2(and breast carcinoma cells (MCF-7) to calculate the cytotoxicity of the prepared compounds. Cell proliferation is inhibited for all compounds and in a dose-dependent manner in the sequence of OVAPPd > OVAPCu > OVAPZn > OVAPCr > OVAP azomethine ligand.

KEYWORDS
anticancer, antioxidant, azomethine complexes, calf thymus DNA interaction, DFT calculations, *In vitro* antimicrobial activity

1 | INTRODUCTION

There has been a considerable increase in the use of metal chelates for cancer treatment after the accidental discovery of the biological activity of platinum complex cisplatin in 1965 by Rosenburg.[1] The organic molecules are designed to combine biological functional groups with a suitable metal ion to mimic active sites of metalloproteins.[2] In recent years, many investigations have been concerned with metal–drug adducts showing promising biological activity and are of great interest in biology and chemistry. Metals like zinc(II), chromium(III) and copper(II) have great affinity for coordination because of their small size and high nuclear charge. The development of metal–drug adducts as chemotherapeutic agents basically depends on the ability of the metallodrug to provoke DNA cleavage.[3–12] It is worth mentioning that metal chelate pharmacological efficacy mainly depends on the nature of metal ions and ligands. The literature suggests that ligands with different metal ions possess different biological properties.[13–21]

Our aim was to undertake a systematic study of the preparation, spectral characterization, DNA binding and biological activities of new transition metal complexes involving the OVAP azomethine ligand 2-[(2-hydroxyphenylimino)methyl]-6-methoxyphenol. The structure of the studied complexes was elucidated using elemental analyses, Fourier transform infrared (FT-IR), ^{1}H NMR, ^{13}C NMR and UV–visible spectroscopies, magnetic moment and molar conductance measurements and thermal analysis and confirmed by density functional theory (DFT) calculations. Moreover, the antimicrobial, antioxidant and cytotoxic effects of the investigated compounds were screened. Furthermore, electronic absorption, viscosity and gel electrophoresis measurements were used to study the ability of the investigated complexes to bind to calf thymus DNA (CT-DNA).

2 | EXPERIMENTAL

2.1 | Reagents

All the chemicals and solvents used in this study were of reagent grade and used as received without additional purification processes. Organic compounds 3-methoxthysalicyaldehyde and 2-aminophenol and metal salts chromium(III) nitrate ($Cr(NO_3)_3{\cdot}6H_2O$), zinc(II) nitrate ($Zn(NO_3)_2{\cdot}4H_2O$), copper chloride ($CuCl_2{\cdot}4H_2O$) and palladium acetate ($Pd(OAC)_2$) were obtained from Sigma-Aldrich.

Ethanol, *N*,*N*′-dimethylformamide (DMF), dimethylsulfoxide (DMSO) and HCl were used without distillation.

The important reagents for DNA interaction studies, CT-DNA, tris(hydroxymethyl)aminomethane (Tris) and EDTA, were obtained from Sigma-Aldrich. CT-DNA was dissolved in Tris–HCl buffer (pH 7.2). Tris–HCl buffer solution was prepared using deionized water and was used to control the pH of reaction systems.

Agarose was purchased from Fischer Biotech (GE Heath Care). Tracking dye (0.20% bromophenol blue, 35% sucrose, 200 mM EDTA and0.20% xylene cyanole) and Ready-load 100 BP DNA ladder were used as the native size DNA and purchased from Bio Labs.

The chemical used for antioxidant activity study, 2,2-diphenyl-1- picrylhydrazyl (DPPH), was purchased from Merck.

To evaluate the antimicrobial activity, bacterial and fungal strains (*Micrococcus luteus* (+ve), *Serratia marcescence* (−ve), *Escherichia coli*, *Pseudomonas aureus*, *Aspergillus flavus*, *Geotrichum candidum* and *Fusarium oxysporum*) were used. These strains were cultured in nutrient agar and Muller-Hinton medium. Ofloxacin and fluconazole were used as standard drugs for comparison.

2.2 | Instrumentation and methods

NMR spectra of the prepared azomethine ligand was measured in DMSO-d_6 and recorded at the Central Laboratory, Department of Chemistry, Faculty of Science, Sohag University at 298 K with a FT-NMR spectrometer (Bruker ARX400) at 400.1 MHz (^{1}H) and 100.6 MHz (^{13}C). Elemental analyses (C, H, N) were performed with a PerkinElmer 2408 CHN analyser at the Micro-analytical Center, Cairo University. Room temperature FT-IR spectra of the prepared azomethine ligand and its complexes were recorded as KBr pellets with a Shimadzu model 8101 FT-IR spectrophotometer in the range 400–4000 cm^{-1} at the Department of Chemistry, Faculty of Science, Sohag University. Electronic spectra were obtained with a Jasco P-530 UV–visible spectrophotometer in DMF at 298 K. Magnetic susceptibilities of the investigated metal azomethine chelates were measured

utilizing the modified Gouy method at 298 K using a magnetic susceptibility balance (Johnson Matthey). An Elico digital pH meter (model LI-127) equipped with a CL-51B combined electrode was used for pH measurements and calibrated against standard buffers (pH 4.02 and 9.18) before measurements. Thermogravimetric analysis (TGA) was conducted using a Shimadzu 60H analyser under air at a heating rate of 10°C min^{-1} from ambient temperature to 750°C at the Department of Chemistry, Faculty of Science, Thermal Analysis Unit, Assiut University, Egypt. DFT calculations were carried out to investigate the equilibrium geometry of the ligand and complexes using the Gaussian 09 program[2] at the B3LYP/LANL2DZ level of theory for the ligand and complexes.

2.3 | Synthesis of OVAP azomethine ligand

The OVAP azomethine ligand was synthesized by a conventional method according to the following procedure. A hot ethanolic solution (10 ml) of 3-methoxthysalicyaldehyde (10 mmol) was added dropwise to another hot ethanolic solution (10 ml) of 2-aminophenol (10 mmol). After completion of addition, a yellow-coloured solid formed on vigorous stirring of the solution. The reaction mixture was refluxed in a water bath for 1 h and then allowed to cool. The completion of the reaction was monitored by TLC.

^{1}H NMR (δ, ppm), in DMSO-d_6:14.01 (1H, OH of phenyl ring), 9.72(s, 1H, OH of methoxy phenyl ring), 8.96 (s, 1H, CH═N), 7.38–6.98(m, 7H, aromatic), 2.50 (3H, CH_3 of methoxy group). ^{13}C NMR (δ, ppm), in DMSO-d_6: 162, 152, 151, 149, 135, 128, 124, 120, 119, 118, 117, 116, 115, 56.

2.4 | Synthesis of OVAP azomethine complexes

To a hot stirred solution of OVAP azomethine ligand (10 mmol) in ethanol (20 ml) was added a solution of metal(II) salt (10 mmol) made in warm ethanol (10 ml) and the resultant mixture was refluxed for 2 h. The solid formed during refluxing or upon cooling was collected by suction filtration. Thorough washing with hot ethanol followed by ether or recrystallization from aqueous ethanol gave purified products.

^{1}H NMR (δ, ppm) of OVAPPd complex in DMSO-d_6: 8.87 (s, 1H, CH═N), 7.99–6.61(m, 7H, aromatic), 2.51 (3H, CH_3 of methoxy group), 3.79 (s, 2H, H_2O).

^{1}H NMR (δ, ppm) of OVAPZn complex in DMSO-d_6: 8.96 (s, 1H, CH═N), 7.39–6.8 (m, 7H, aromatic), 2.51 (3H, CH_3 of methoxy group), 3.84 (s, 2H, H_2O). ^{13}C NMR (δ, ppm) of OVAPZn complex in DMSO-d_6: 162, 152.5, 151, 149, 135, 128.5, 124, 120, 119, 118, 117, 116, 115.5, 56.4.

2.5 | Determination of stoichiometry

Job's method (continuous variation method)[22–26] was used to determine the stoichiometry of the investigated complexes. A mixture of metal salt and ligand solution was mixed, stirred and left to equilibrate, and the absorbance measured at λ_{max} up to 2 h. The absorbance of each solution was then plotted against the mole fraction of metal ion or mole fraction of ligand.

2.6 | Kinetic parameters for TGA of the prepared complexes

The decomposition and thermal dehydration of the metal chelates were studied kinetically using the integral method applying the Coats–Redfern method. Moreover, the thermodynamic activation parameters of degradation steps of dehydrated complexes, namely energy of activation (E), frequency factor (A), enthalpy of activation (ΔH), entropy of activation (ΔS) and free energy change of the decomposition (ΔG), were evaluated from TGA data graphically utilizing the Coats–Redfern relation[6–10,27–30] in the following form:

$$\log\left[\frac{\log(W_\infty/(W_\infty - W))}{T^2}\right] = \log\left[\frac{AR}{\varphi E^*}\left(1-\frac{2RT}{E^*}\right)\right] - \frac{E^*}{2.303RT} \quad (1)$$

where W_∞ is the mass loss at the completion of the decomposition reaction, W is the cluster loss up to temperature T, R is the general gas constant and ϕ is the heating rate. Since $1 - 2RT/E^* \approx 1$, a plot of the left-hand side of equation (1) against $1/T$ would give a straight line. E^* was calculated from the slope and the Arrhenius constant, A, was determined from the graph intercept. The other kinetic parameters, namely the entropy of activation (ΔS^*), enthalpy of activation (ΔH^*) and free energy change of activation (ΔG^*), were calculated using the following equations:

$$\Delta S^* = 2.303R\log\frac{Ah}{K_B T} \quad (2)$$

$$\Delta H^* = E^* - RT \quad (3)$$

$$\Delta G^* = \Delta H^* - T\Delta S^* \quad (4)$$

where K_B and h are the Boltzmann and Planck constants, respectively.

2.7 | Investigation of DNA interaction with azomethine metal chealates

All DNA binding experiments were done in 10 mM Tris–HCl buffer (pH = 7.4) containing 50 mM NaCl. A solution of CT-DNA gave a ratio of UV absorbance at 245 and 262 nm of greater than 1.8, indicating that the DNA was adequately free from protein.[15–17,31,32] Molecular absorption spectroscopic experiments were executed at 25°C, maintaining the concentration of each metal chelate constant (10.0 μM) while altering the concentration of DNA from 0 to 15.0 μM. After each addition of DNA to the metal complex, the resulting solution was allowed to equilibrate at 25°C for 10 min, after which the change in absorbance of the ligand-to-metal charge transfer band was recorded. While measuring the absorption spectra, an appropriate amount of CT-DNA in Tris–HCl buffer solution (pH = 7.4) was added to both metal chelate solution and the blank reference to eliminate the absorption of CT-DNA itself. The intrinsic binding constant (K_b) was determined by way of plotting [DNA]/($\varepsilon_a - \varepsilon_f$) versus [DNA] according to the following expression:[29,32,33]

$$\frac{[DNA]}{(\varepsilon_a - \varepsilon_f)} = \frac{[DNA]}{(\varepsilon_b - \varepsilon_f)} + \frac{1}{[K_b(\varepsilon_b - \varepsilon_f)]} \quad (5)$$

where [DNA] is the concentration of DNA in base pairs and ε_a, ε_f and ε_b are the apparent, free and completely bound metal chelate eradication coefficients, respectively. Specifically, ε_f was assessed from the calibration curve of the separated metal chelate; confirmation of Beer's law. ε_a was assessed as the proportion among the determined absorbance and the M(II) chelate concentration, A_{obs}/(metal chelate). The information became reasonable for the above equation with a slope equivalent to $1/(\varepsilon_b - \varepsilon_f)$ and y-intercept equivalent to $1/(K_b(\varepsilon_b - \varepsilon_f))$; K_b was obtained from the ratio of slope to intercept. The standard Gibbs free energy for DNA binding was assessed from the following expression:

$$\Delta G_b^{\neq} = -RT \ln K_b \quad (6)$$

Hydrodynamic measurements (viscosity) were executed utilizing an Ostwald viscometer at room temperature using 20 μM CT-DNA, complex concentrations of 0 to 100 μM and measuring the flow times with a digital timer. Each sample was measured three times for accuracy, and an average flow time was calculated. Data were presented as $(\eta/\eta_0)^{1/3}$ versus [complex]/[DNA], where η is the viscosity of DNA in the presence of metal chelate and η_0 is that of DNA alone. The values of viscosity were calculated from the flow time of DNA-containing solutions (t) with subtraction of that of only buffer solution (5 mM Tris–HCl/50 mM NaCl) (t_0): $\eta = (t - t_0)$.

The cleavage efficiency of prepared azomethine metal complexes with calf thymus DNA was examined by the gel electrophoresis method. Hot Tris–acetate–EDTA (TAE) buffer (50 ml) (4.84 g of Tris base, pH = 8.0, 0.5 M EDTA) was used to dissolve agarose (500 mg) then heated until boiling for a few minutes. When the gel reached approximately 55°C, it was poured into a gas cassette fitted with comb. After that, the gel was left to solidify slowly by cooling to room temperature and then the comb was removed carefully. Then gel in a solid form was placed in the electrophoresis chamber including TAE buffer. The prepared metal chelate samples were subjected to electrophoresis on 2% agarose gel prepared in TBE buffer (45 mM boric acid, 45 mM Tris and 1 mM EDTA, pH 7.1). Then 20 μl of each of the incubated metal chelates and 20 μl of DNA were used. The resulting mixture was incubated for 25 min at 37°C. After that, it was loaded with tracking dye (0.30% bromophenol blue) on the prepared gel. The electric current was turned off at the end of migration of DNA. Ethidium bromide solution in water (0.5 μg ml^{-1}) was used to stain the gel for 40 min at room temperature and later the gel was visualized under UV light utilizing a transilluminator. The illuminated gel was photographed using a Panasonic digital camera.

2.8 | Antimicrobial assessment

The antimicrobial activity of the free ligand and its corresponding metal complexes were primarily screened against pathogenic bacteria and fungi that are common contaminants of the environment in Sohag, Egypt, and some of which are involved in human and animal diseases, such as *Aspergillus flavus*, *Geotrichum candidum* and *Fusarium oxysporum*, or frequently reported from contaminated soil, water and food substances, e.g. *Serratia marcescence*, *Escherichia coli* and *Micrococcus luteus*. *In vitro* biological activities of OVAP azomethine ligand and its metal chelates in DMSO medium were investigated for their microbial inhibition using standard agar as the medium using the a well diffusion method.[29,32–34] Wells were set up in cooled agar plates (1 cm). An amount of 10 mg of each compound was dissolved in 3 ml of DMSO and 100 μl was loaded in a well. The activity or sensitivity was observed after 24–48 h incubation at 37°C. The minimum inhibitory concentration (MIC) ranges were determined. Zone of inhibition of the investigated metal complexes was compared with that of available standard

drugs.[33,35] The MIC is the smallest concentration of compound that inhibits the growth of microorganisms.

2.9 | Antioxidant assay (DPPH free radical scavenging activity)

In vitro antioxidant activity of the newly synthesized OVAP azomethine ligand and its metal complexes was evaluated using a modified stable DPPH radical scavenging method.[32] The stable DPPH radical scavenging method is used to determine antioxidant activities of the prepared compounds in a relatively short time compared with other methods. The change of absorption, easily observed as a colour change from purple to yellow, of the radical when deactivated by antioxidant is a reliable test in the DPPH radical scavenging model. Methanol–DMSO (4:1) stock solutions of the investigated compounds were prepared then diluted to final concentrations of 10, 25, 50, 100 and 150 M. A (1 ml, 0.3 mmol) methanolic solution of DPPH was added to 3.0 ml of the synthesized compounds as well as standard compound (ascorbic acid). Each tube was kept in the dark for 30 min and the absorbance was measured in triplicate at 517 nm using methanol as a blank. The positive control was vitamin C. The reduction in the absorbance of DPPH was calculated relative to the measured absorbance of the control. The DPPH radical scavenging percentage of activity was calculated using the following equation:

$$\text{DPPH scavenging activity } (\%) = \frac{A_C - A_S}{A_C} \qquad (7)$$

where A_C is the absorbance of vitamin C (standard) and A_S is the absorbance of sample under investigation. The effective concentration of sample required to scavenge DPPH radicals by 50% (IC50 value) was obtained by linear regression analysis of dose–response curve plotting between percent inhibition and concentration.

2.10 | Cell culture and experimental conditions

Cancer cell lines were cultured in RPMI 1640 medium in culture flasks, supplemented with 10% foetal bovine serum and 100 μg ml^{-1} penicillin and streptomycin. Cancer cells were incubated at 37°C in a 5% CO_2-supplemented atmosphere for at least 24 h before the appropriate treatments and used to determine the cell viability against the synthesized compounds.

2.10.1 | Cytotoxicity by MTT assay

The viability of cancer cells against the synthesized compounds was examined using MTT assay as previously described.[36,37] Colon carcinoma cells (HCT-116), hepatic cellular carcinoma cells (HepG-2) and breast carcinoma cells (MCF-7) were seeded in 96-well plates at a density of 5×10^3 cells per well. After 24 h they were exposed to different concentrations of compounds (ranging between 0 and 10 μg ml^{-1}) for 48 h. After the treatment, the medium containing the compounds was removed and 10 μl of MTT (5 mg ml^{-1} in phosphate-buffered saline) was added to each well and incubated at 37°C for 3 h. Then, 100 μl of DMSO was added to dissolve the purple crystals. The optical density values of wells were measured at 570 nm. Each concentration was tested three times and five replica wells were used for controls and 5-fluorouracil was used as standard drug. With the control wells representing 100% viability, the absorption values of each well were expressed as the percentage cell viability. C_{50} values were calculated from the dose–response curves using Origin software, representing the concentration of test compound to inhibit cell viability by 50%. Every concentration for each compound was tested in triplicate and mean values ± SD were recorded.

3 | RESULTS AND DISCUSSION

3.1 | Identification of prepared compounds

The obtained solid complexes are coloured and quite stable in air and moisture (Scheme 1). The complexes were found to have ligand-to-metal ratio of 1:1. Table 1 presents all the analytical and physical data of the OVAP azomethine ligand and its metal chelates. Good agreement between the elemental analyses with the chemical formulae of the proposed structures of the prepared compounds was observed. FT-IR, ^{1}H NMR, ^{13}C NMR and mass spectra and microanalyses were used to elucidate the structure of OVAP azomethine ligand and its metal chelates formed as well as the coordination mode of the ligand.

3.1.1 | IR spectra and mode of bonding for prepared OVAP azomethine ligand and its complexes

In order to authenticate the formation of ligand and metal complexes, the FT-IR spectra of OVAP azomethine ligand and its metal chelates are discussed (Figures S1 and S2; and Table 1). A comparative study of their FT-IR spectra indicates that certain peaks are of interest.

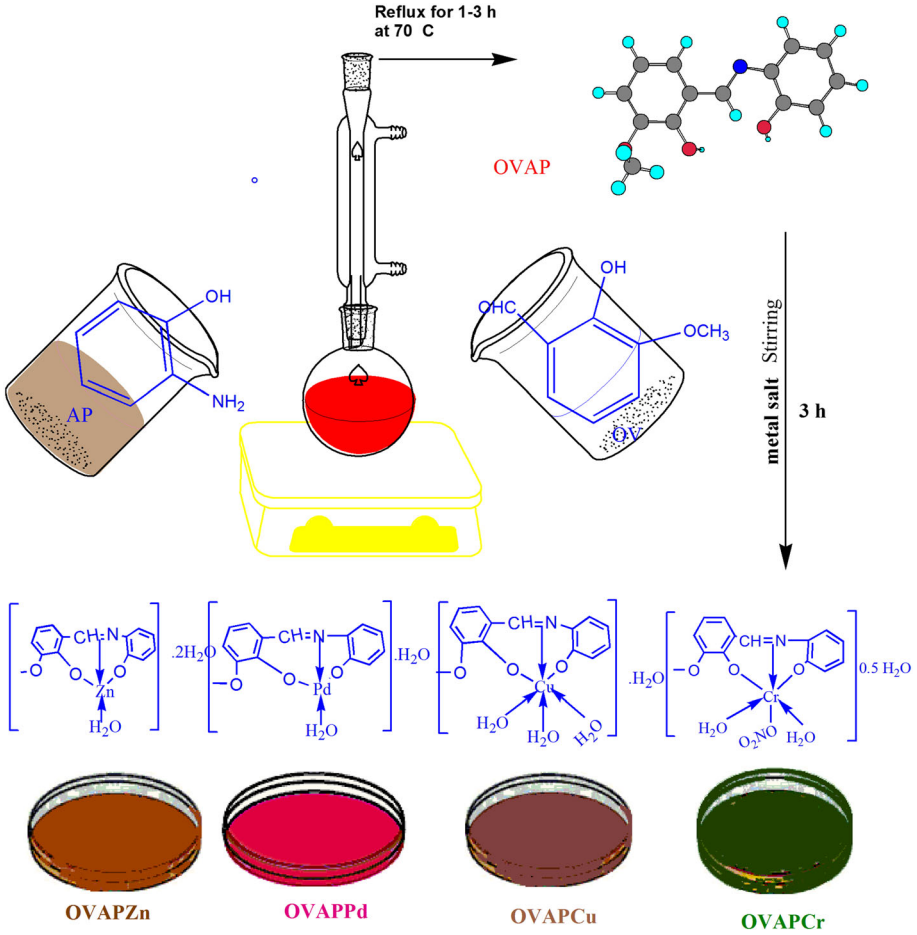

SCHEME 1 Synthetic strategy for preparation of the investigated complexes

Thus, only important peaks that are shifted or have newly appeared are discussed. The band at 1628 cm^{-1} in the FT-IR spectrum at of OVAP ligand corresponds to ν(HC═N) group. In the FT-IR spectra of the metal complexes, it was observed that the band undergoes a blue shift to lower values by 16–27 cm^{-1}, which implies the formation of a bond between nitrogen of azomethine group and metal ion and a reduction of the double bond character of carbon–nitrogen bond.[38–41] Supporting that, new bands due to ν(M—N) bond appeared in the range 442–494 cm^{-1}. The broad band corresponding to ν(—OH) stretching vibrations, which appeared at 3376 cm^{-1} for the ligand, disappeared after complex formation, pointing to the deprotonation of phenolic OH during complex formation.[42,43] This is further supported by the appearance of new bands due to metal–oxygen bond formation in the region 529–562 cm^{-1}.[44] Broad bands in the region 3378–3423 cm^{-1} point to the presence of coordinated water molecules in the complexes. This is further supported by the presence of bands corresponding to ν(—OH) rocking and wagging mode of vibrations at 737–742 cm^{-1}.[45] In the spectrum of the Cr(III) complex, new peaks appeared as a result of binding of nitrate group inside the coordination sphere. The characteristic frequencies of the coordinating nitrate group in the Cr(III) complex shows three non-degenerate modes at 1430 cm^{-1} of $\nu(NO_2)_{asy}$, 1384 cm^{-1} of $\nu(NO_2)_{sy}$ and 828 cm^{-1} of ν(NO).[46] Based on these spectral observations, we conclude that OVAP azomethine ligand coordinates in a bi-negative tridentate manner around the Cr(III), Zn(II), Cu(II) and Pd(II) metal ion centres.

3.1.2 | ^{1}H NMR, ^{13}C NMR and mass spectra of prepared OVAP azomethine ligand and its diamagnetic complexes

To investigate the encapsulation behaviour, ^{1}H NMR and ^{13}CNMR studies were used for demonstrating the interaction of the host molecule and guest molecule between OV and AP. The ^{1}H NMR and ^{13}C NMR results are displayed in Figure S2 (supporting information) and detailed in section 2.

The ^{1}H NMR spectrum of OVAP azomethine ligand (Figure 1) demonstrated singlet signals at 14.01 and 9.72 ppm which were attributed to proton hydroxyl group

TABLE 1 Prepared azomethine OVAP ligand and its complexes, abbreviations, molecular formulae, melting points, decomposition temperatures, elemental analyses and characteristic FT-IR bands

Compound	Empirical formula (formula weight)[a]	Colour	(M.p.) and decomp. temp. (°C)	Λ_m (Ω^{-1} cm^2 mol^{-1})	μ_{eff} (BM)	Analysis: found (calcd)			IR, Cm^{-1}				
						C (%)	H (%)	N (%)	(υOH)/ H_2O	υ(C=N (vs))	υ(C–O) ph	υ(M–O)	υ(M–N)
OVAP	$C_{14}H_{13}NO_3$ (243.26)	Deep red	175	—	—	69.21 (69.12)	5.45 (5.39)	5.69 (5.76)	3376	1628	1277		
OVAPCr	$[Cr(C_{14}H_{16}N_2O_9)]$ (400.27)	Deep green	> 300	9.25	3.78	41.92 (41.97)	4.04 (3.99)	6.95 (6.99)	3380	1601	1253	529	488
OVAPPd	$[Pd(C_{14}H_{15}NO_5)]$ (383.69)	Light red	> 300	6.50	—	43.90 (43.82)	3.98 (3.94)	3.62 (3.65)	3423	1603	1226	538	442
OVAPCu	$[Cu(C_{14}H_{19}NO_7)]$ (376.85)	Deep brown	> 300	11.60	2.09	44.68 (44.62)	5.12 (5.08)	3.69 (3.72)	3378	1611	1228	524	494
OVAPZn	$[Zn(C_{14}H_{17}NO_6)]$ (360.68)	Brown	> 300	8.50	—	46.66 (46.62)	4.72 (4.75)	3.84 (3.88)	3421	1612	1224	562	459

[a]Formula weight in g mol^{-1}.

of phenyl ring and methoxy of phenyl ring, respectively. Also it shows a singlet signal at 8.96 ppm, which was assigned to the azomethine group. Also, it displays multiplet signals at 7.38–6.98 ppm for seven aromatic CH for the two rings in the ligand. Also, it displays a singlet signal at 2.50 ppm due to 3H protons of methoxy group. The ^{13}C NMR spectrum of OVAP ligand (Figure S3) displayed a signal at 162.00 ppm which probably corresponded to azomethine carbon. The signals in the range 152–115 ppm were assigned to phenyl carbons as demonstrated in Figure S3. Furthermore it displays singlet signal at 56 ppm due to aliphatic carbon of methoxy group.

The ^{1}HNMR spectrum of OVAPPd complex clearly demonstrates the presence of the framework protons of the OVAP molecule. It shows a singlet signal at 8.37 ppm which assigned to the proton of azomethine group. Moreover, it shows multiplet signals at 7.99–6.61 ppm for aromatic 7-CH protons (Figure S4 and section 2). Additionally, it displays a singlet signal at 2.51 ppm due to 3H protons of methoxy group. Furthermore, the OVAPPd complex shows a singlet signal at 3.79 ppm attributed to the two protons of H_2O molecule.

The ^{1}H NMR spectrum of the OVAPZn complex clearly demonstrates the presence of the framework protons of the OVAP molecule. It shows a singlet signal at 8.96 ppm which was assigned to the proton of azomethine group. Moreover, it shows multiplet signals at 7.39–6.8 ppm for aromatic 7-CH protons (Figure S5 and section 2). Also, it displays a singlet signal at 2.51 ppm due to 3H protons of methoxy group. Furthermore, the OVAPZn complex shows a singlet signal at 3.84 ppm, attributed to the two protons of H_2O molecule. Thus the formation of OVAP ligand and its complexes with the proposed chemical structures was established. The ^{13}C NMR spectrum of OVAPZn complex exhibits resonances with slight chemical shifts (Figure S6 and section 2).

The ESI mass spectrum of ligand OVAP, for further structural information, is given in Figure S7. The spectrum shows the molecular ion peak at m/z 244 and the isotopic peak at m/z 244 (M^+) due to the presence of ^{13}C and ^{15}N isotopes. The base peak at m/z 228 is due to $(C_{14}H_{12}NO_2)^+$ ion. Another intense peak at m/z 120 is due to $(C_7H_4O_2)^+$ ion. The intensity of these peaks reflects the stability and abundance of the ions.

3.1.3 | Electronic spectra, conductivity measurements and magnetic moments for OVAP azomethine ligand and its metal chelates

Electronic spectra of the investigated complexes were measured in DMF as solvent. The highest energy band is

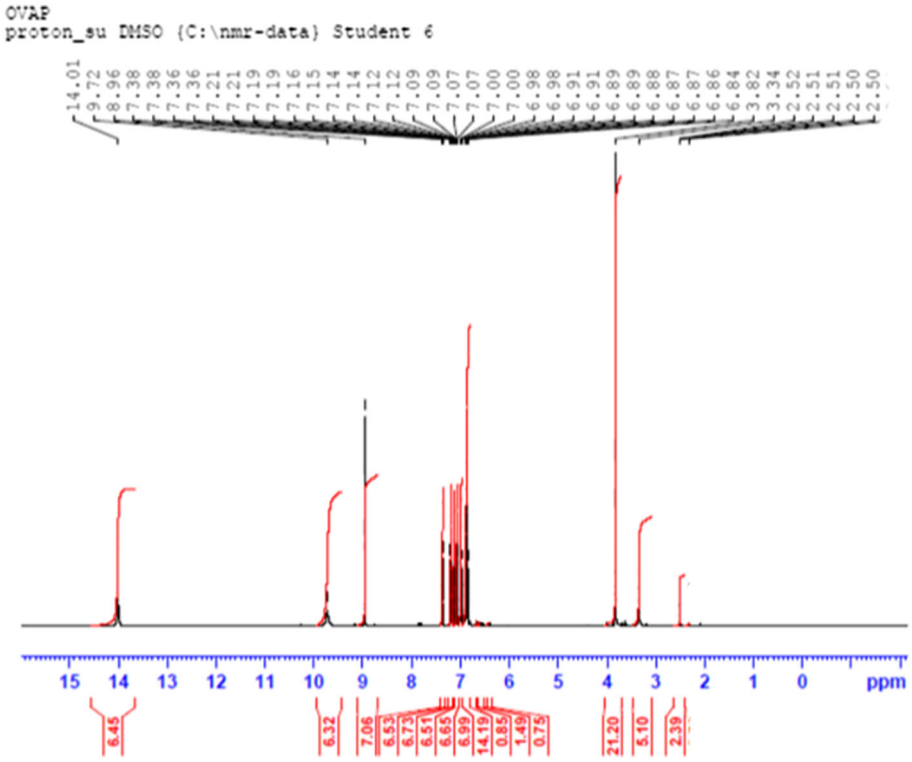

FIGURE 1 ^{1}H NMR spectrum of OVAP ligand

assigned to π–π* transition while the shoulder may be assigned to an intramolecular charge transfer. OVAP azomethine ligand exhibits absorption bands in the UV–visible region at 288 and 350 nm which are assigned to n → π* transition originating from the azomethine function of the ligand which is shifted on complexation. The absorption bands of complexes at λ_{max} = 318–490 nm are assigned to charge transfer transitions. These transitions probably occur from the p-orbitals of the azomethine to the d-orbitals of the metal ions. The appearance of a low-intensity broad band lying in the region 430–520 nm in the electronic spectra of the complexes that is absent in the spectrum of the free ligand is further evidence of the complexation process. This band could be mainly ascribed to the d → d transition in the structure of the investigated metal chelates. Since zinc ion has a d^{10} configuration, diamagnetic, the observed absorption spectra of the Zn(II) complex could be assigned in terms of the absence of any d–d electronic transitions (cf. Figure 2).

The molar conductance (Λ_M) values for the prepared complexes are found in the range 6.5–11.6 $cm^2\ \Omega^{-1}\ mol^{-1}$, indicating a non-electrolytic nature and there is no counter ion present outside the coordination spheres of the complexes. So, we conclude that all the prepared complexes are neutral in nature.[38,43,47]

The magnetic moment for complexes is generally diagnostic of the coordination geometry about the metal ion.

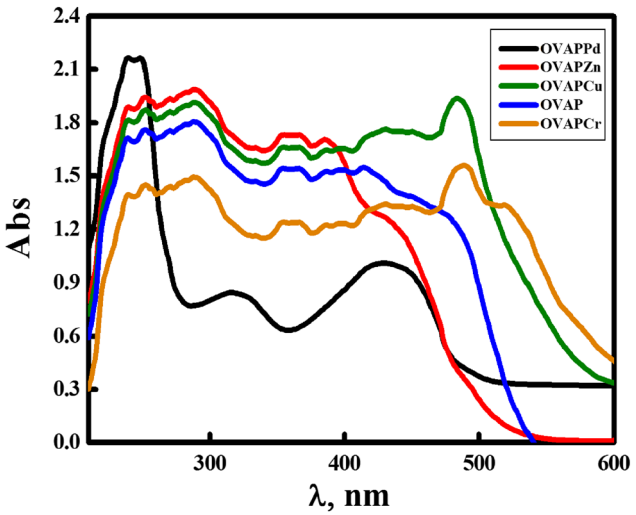

FIGURE 2 Molecular electronic spectra of of OVAP azomethine ligand and its complexes in DMF (10^{-3} M) at 298 K

Orbital contribution is the reason for the variation of spin-only value that varies with the nature of coordination and consequent delocalization. Diamagnetic behaviour with zero μ_{eff} value of OVAPPd and OVAPZn complexes suggests that they have square planar and tetrahedral geometry, respectively.[48] The magnetic moment value observed for the OVAPCr complex is 3.78 BM, and is close to theoretical spin-only values for Cr^{3+} ($3d^3$ system) of octahedral geometry.[20] Magnetic susceptibility value of

the OVAPCu complex is 1.87 BM, which suggests a distorted octahedral geometry for the Cu(II) ion.[49]

The Nujol mull spectrum of the OVAPCr complex showed two bands at 18 781 and 27 415 cm^{-1} which can be assigned to $^4B_{1g} \rightarrow {}^4E^a_g$ and $^4B_1g \rightarrow {}^4E^bg$ transitions, respectively, reinforcing the lifting of the degeneracy of the orbital triplet (in octahedral symmetry).[20] The band at 28 822 cm^{-1} in the spectrum of the OVAPPd complex is assignable to a combination of, for example, (d_{yz}, d_{zx})–b_{1g} $(dx^2–y^2)$, i.e.$^1A_{1g} \rightarrow {}^1E_g$ and metal-to-ligand charge transfer indicating a square planar geometry.[48,50,51] The electronic spectrum of the Cu^{2+} complex displayed a band at 17 790 cm^{-1} assigned to $^2E_g \rightarrow {}^2T_{2g}$ transition indicative of octahedral geometry around the Cu(II) ion.[49,52] The electronic spectrum of the OVAPZn complex, as d^{10} system, exhibited a non-ligand band at 21 217 cm^{-1}, corresponding to ligand-to-metal charge transfer transition. The clear shifts in the Schiff base bands are indicative of complex formation.[53,54]

3.1.4 | TGA of prepared azomethine complexes

The metal complexes show similar decomposition patterns as evident from their TGA curves (Figure S8).

The characteristic thermogram of OVAPCu shows five distinct mass losses up to 640°C. Dehydration of one water molecule in the first step up to 110°C is followed by removal of three coordinated water molecules up to 187°C. During further heating, a complete decomposition of the OVAPCu azomethine complex in three steps occurs with mass losses of about 8.22% (calcd 8.23%), 24.20% (calcd 24.15%) and 27.31% (calcd 27.35%) in the temperature ranges 189–301, 303–379 and 381–640°C, respectively, leaving a residue of CuO.

The thermogram of OVAPPd shows loss in weight within the range 36–112°C, which is due to removal of the hydrated water molecule (found 4.57%, calcd 4.67%) followed by loss of one coordinated water molecule within the range114–191°C. Also, it shows three mass losses within the range 193–730°C, which is due to removal of ligand moiety leaving PdO as a final residue.

The characteristic thermogram of OVAPZn shows five distinct mass losses up to 697°C. In the first step up to 110°C, it dehydrates two water molecules followed by removal of one coordinated water molecule up to 185°C. During further heating, the OVAPZn complex undergoes complete decomposition in three steps and shows mass losses of about 8.62% (calcd 8.59%), 25.19% (calcd 25.23%) and 28.63% (28.56%) up to 697°C of the ligand moiety leaving ZnO as a residue.

The thermogram of OVAPCr shows five decomposition steps within the range 36–618°C. Within the range 36–115°C, a decomposition step corresponds to the loss of half a hydrated water molecule with a mass loss of 2.27% (calcd 2.25%). A second step of decomposition within the range 117–295°C corresponds to the loss of nitrate and two coordinated water molecules with a mass loss of 24.22% (calcd 24.25%). The third step up to 330°C with mass loss of 7.76% (calcd 7.75%) indicates the removal of the methoxy group part of the azomethine ligand (OCH_3). The fourth step in the range 332–505°C, with an estimated mass loss of 20.71% (calcd 20.75), corresponds to loss of part of the azomethine ligand ($C_6H_3O_{0.5}$) followed by removal of the remaining part of the ligand (C_7H_5N) up to 618°C leaving Cr_2O_3 as a residue. The TGA data (Table 2) show good agreement with the suggested stoichiometry abstracted from findings of elemental analysis.

3.1.5 | Kinetic and thermodynamic studies

Table 2 presents the thermodynamic activation parameters from the Coats–Redfern graphical evaluation method, namely the activation energy (ΔE^*), entropy (ΔS^*) and Gibbs free energy change of decomposition (ΔG^*), of the Cr(III), Zn(II), Cu(II) and Pd(II) complexes. Form the obtained data, the following observations can be summarized:

i. The ΔS^* values for the complexes were found to be negative. This implies that the activated complex is more ordered than starting materials and/or the reactions are slow.[55,56]
ii. The negative values of ΔH^* means that the decomposition processes are exothermic.
iii. The positive values of ΔG^* for the investigated complexes increases significantly for the subsequent degradation steps due to increasing values of $T\Delta S^*$ from one step to another which override the values of ΔH^*. This increase indicates that the rate of removal of the subsequent azomethine ligand will be slower than that of the preceding ligand.[57]

TABLE 2 Formation constant (K_f), stability constant (pK) and Gibbs free energy (ΔG^*) values of the synthesized azomethine complexes at 298 K

Complex	Type of complex	K_f	Log K_f	ΔG^* (kJ mol^{-1})
OVAPPd	1:1	2.62×10^4	4.41	−25.20
OVAPCr	1:1	4.15×10^4	4.61	−26.33
OVAPCu	1:1	1.28×10^4	4.11	−23.42
OVAPZn	1:1	3.85×10^4	4.58	−26.15

3.1.6 | Stoichiometry determination for prepared complexes utilizing spectrophotometric method

Based on the methods which were utilized and the experimental data, the stoichiometry of the prepared metal chelates is 1:1. The curves of the continuous variation method (Figure 3) give a maximum absorbance at mole fraction X_{ligand} = 0.5–0.6, showing the complexation of metal ions to OVAP azomethine ligand in a molar ratio of 1:1. Moreover, the data resulting from utilizing the molar ratio method support the same metal ion to ligand ratio of the prepared complexes (Figure S9).[22–26]

3.1.7 | Formation and stability constants for investigated complexes

Spectrophotometric measurements utilizing the continuous variation method were used to determine the formation constants (K_f) of the resultant azomethine complexes which formed in solution (Table 3). The estimated K_f values show the high stability of the complexes. The order of decreasing values of K_f is as follows: OVAPCr > OVAPZn > OVAPPd > OVAPCu. Moreover, the values of the stability constant (pK) and Gibbs free energy ($\Delta G^{\neq}$) of the complexes were calculated. The observed negative values of Gibbs free energy give an indication of the spontaneous complexation reaction. The diagram for stability of the investigated metal chelates at different pH values (Figure 4) shows typical dissociation curves and a high pH stability range (5–11) of the metal chelates.

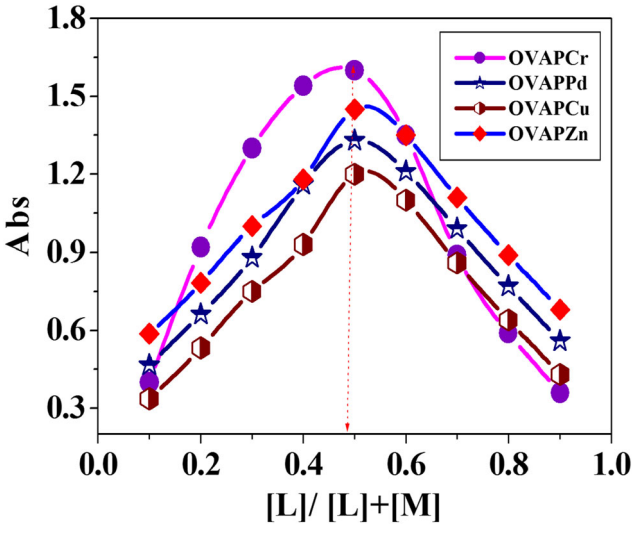

FIGURE 3 Continuous variation plots for the prepared OVAPCr, OVAPV, OVAPZn and OVAPCu complexes in aqueous–ethanolic medium at [OVAPCr] = [OVAPPd] = [OVAPZn] = [OVAPCu] = 10^{-3} M and 298 K

This indicates that the formation of the complex greatly stabilizes the OVAP aazomethine ligand. Consequently, the optimum pH range for different applications of the complexes is from pH = 5 to 11. Correlation between the data obtained from elemental analyses, molar conductance and magnetic measurements, infrared and electronic spectra and the suggested composition of the complexes was identified.

3.2 | Molecular DFT calculation for OVAP azomethine ligand and its complexes

3.2.1 | Molecular DFT calculation of OVAP azomethine ligand

Figure 5 shows the optimized structures of OVAP as the lowest energy configurations. The natural charges obtained from natural bond orbital (NBO) analysis show that the more negative active sites are in the order O1 (−0.731) > O3 (−0.729) > O2 (−0.601) > N1 (−0.545). The metal ions prefer tridentate coordination to O1, O3 and N1 forming five- and six-membered rings.

3.2.2 | Molecular DFT calculation of OVAP ligand and [Cu(OVAP)(H_2O)$_3$] complex

Figure 6 shows the optimized structures of the [Cu(OVAP)(H_2O)$_3$] complex as the lowest energy configurations. The copper atom is six-coordinate in a distorted octahedral geometry with O4 and O5 of water molecules being in axial positions. The dihedral angles of atoms in the three perpendicular planes O1, N1, O3 and O6 (−1.023°), N1, O4, O6 and O5 (3.661°) and O1, O5, O3 and O4 (−4.364°) indicate that these atoms are almost in one plane. The bond angles in the octahedral geometry range from 84.89° to 95.04° (Table 4). The distances between donor atoms O1···N1 and O1···O3 involved in coordination are largely decreased upon complex formation from 4.024 and 6.616 Å (in free ligand) to 2.912 and 3.914 Å (in the complex), respectively (Table 4).

The natural charges computed from the NBO analysis on the coordinated atoms are Cu (+0.992), O1 (−0.771), N1 (−0.578), O3 (−0.724), O4 (−0.941), O5 (−0.933) and O6 (−0.934) (Figure 6).

3.2.3 | Molecular DFT calculation of [Cr(OVAP)NO_3(H_2O)$_2$] complex

Figure 7 shows the optimized structures of the [Cr(OVAP)NO_3(H_2O)$_2$] complex as the lowest energy

TABLE 3 Thermal decomposition steps, mass loss, proposed lost segments, final residue and thermo-kinetic activation parameters of each decomposition step for the prepared complexes

Complex	Decomp. temp. (°C)	Mass loss (%) Found	(Calcd)	Proposed segment	E^* (kJ mol^{-1})	A (s^{-1})	ΔH^* (kJ mol^{-1})	ΔG^* (kJ mol^{-1})	ΔS^* (J mol^{-1} K^{-1})
OVAPCu	35–110	4.75	(4.78)	H_2O	28.50	0.082	27.90	46.20	−253.93
	112–187	14.36	(14.33)	$3H_2O$			27.20	66.20	−260.04
	189–301	8.22	(8.23)	CH_3O			26.46	91.20	−264.12
	303–379	24.20	(24.15)	C_6H_3O			25.70	116.70	−266.86
	381–640	27.31	(27.35)	C_7H_5N			24.30	162.10	−270.21
Residue	> 640	21.09	(21.11)	CuO			—	—	—
OVAPPd	36–112	4.57	(4.69)	H_2O	25.40	0.022	24.80	44.40	−265.10
	114–191	4.63	)4.69)	H_2O			24.10	65.30	−271.09
	193–340	8.12	)8.08)	CH_3O			23.20	96.50	−275.74
	342–527	23.76	)23.72)	C_6H_3O			21.80	143.20	−279.81
	529–730	26.89	)26.84)	C_7H_5N			20.20	198.40	−282.91
Residue	>730	31.96	(31.90)	PdO			—	—	—
OVAPZn	35–110	9.99	(9.98)	$2H_2O$	30.10	0.074	29.50	48.10	−254.90
	112–185	4.97	(4.99)	H_2O			28.90	67.50	−260.78
	187–346	8.62	(8.59)	CH_3O			27.90	98.80	−265.69
	348–549	25.19	(25.23)	C_6H_3O			26.40	147.90	−270.02
	551–697	28.63	(28.56)	C_7H_5N			24.90	195.10	−272.74
Residue	35–110	22.57	(22.56)	ZnO			—	—	—
OVAPCr	36–115	2.27	(2.25)	0.5 H_2O	49.80	0.49	49.20	67.20	−239.41
	117–295	24.22	(24.50)	$2H_2O + NO_3$			48.10	99.10	−247.81
	297–330	7.76	(7.75)	CH_3O			47.20	125.90	−251.29
	332–505	20.71	(20.75)	$C_6H_3O_{0.5}$			46.30	152.30	−253.69
	507–618	25.74	(25.75)	C_7H_5N			45.10	189.10	−256.15
Residue	> 618	18.97	(19.00)	$0.5Cr_2O_3$					

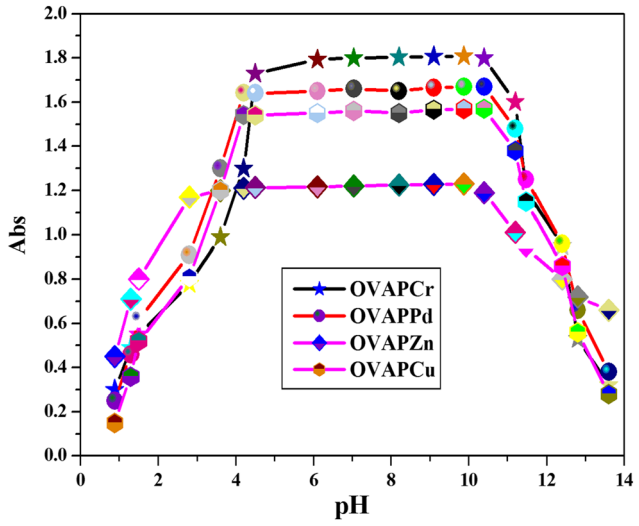

FIGURE 4 Dissociation curves of the prepared OVAPCr, OVAPPd, OVAPZn and OVAPCu complexes in DMF

configurations. The chromium atom is six-coordinate in a distorted octahedral geometry with O7 and O8 of water molecules in axial positions. The dihedral angles of atoms in the three perpendicular planes N1, O7, O4 and O8 (0.378°), O3, O8, O1 and O7 (13.12°) and O1, N1, O3 and O4 (−9.251°) indicate that these atoms are almost in one plane. The deviation may be attributed to hydrogen bonding and the restriction caused by the tridentate ligand. The bond angles in the octahedral geometry range from 78.96° to 97.54° (Table 5). The distances between donor atoms O1···N1 and O1···O3 involved in coordination are largely decreased upon complex formation from 4.024 and 6.616 Å (in free ligand) to 2.713 and 3.661 Å (in the complex), respectively (Table 5). Also, the bond angle of C7–N1–C8 is smaller in the complex (122.8°) compared to in the free ligand (130.1°) due to complex formation. The natural charges computed from the NBO analysis on the coordinated atoms are Cr (+0.714), O1 (−0.543), N1 (−0.451), O3 (−0.610), O4 (−0.467), O7 (−0.865) and O8 (−0.876) (Figure 7).

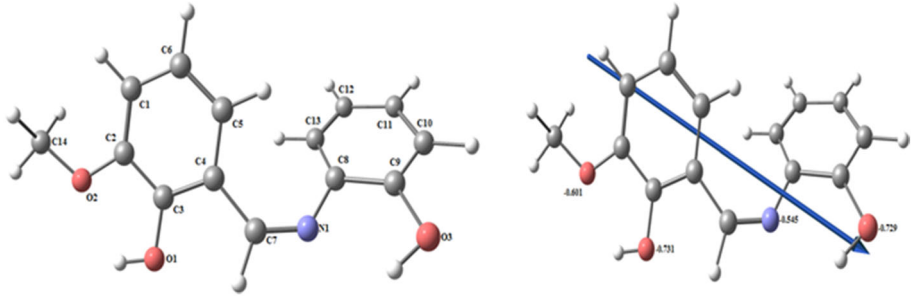

FIGURE 5 Optimized structure of OVAP, vector of dipole moment, and natural charges on active centres of OVAP by density function B3LYP/LANL2DZ

TABLE 4 Important optimized bond lengths (Å) and bond angles (°) of OVAP and [Cu (OVAP)$(H_2O)_3$] complex

Type of bond	Bond length(Å) Complex	Type of bond	Bond length(Å) OVAP	Complex
Cu–N1	2.073	Cu–O5	—	2.237
Cu–O1	1.960	Cu–O6	—	2.135
Cu–O3	1.956	O1···N1	4.024	2.912
Cu–O4	2.251	O1···O3	6.616	3.914
Type of angle	**Angle (°) Complex**	**Type of angle**	**Angle (°) Complex**	
N1–Cu–O1	92.43	O5–Cu–O1	88.70	
N1–Cu–O3	84.89	O5–Cu–O3	93.43	
O1–Cu–O6	87.63	O5–Cu–O6	88.32	
O3–Cu–O6	95.04	N1–Cu–O6	179.5	
O4–Cu–N1	91.76	O1–Cu–O3	176.6	
O4–Cu–O1	86.25	O4–Cu–O5	173.7	
O4–Cu–O3	91.79	O1–N1–O3–O6	−1.023[a]	
O4–Cu–O6	87.75	N1–O4–O6–O5	3.661[a]	
O5–Cu–N1	92.18	O1–O5–O3–O4	−4.364[a]	

[a]Dihedral angle.

3.2.4 | Molecular DFT calculation of [Pd(OVAP)H_2O] complex

Figure 8 shows the optimized structures of the [Pd(OVAP)H_2O] complex as the lowest energy configurations. The palladium atom is four-coordinate in a distorted square planar configuration with atoms O1, N1, O3 and O4 almost in one plane deviating by −0.380°. The bond angles in the square planar geometry range from 83.50° to 96.56° (Table 6). The distances between donor atoms O1···N1 and O1···O3 involved in coordination are largely decreased upon complex formation from 4.024 and 6.616 Å (in free ligand) to 2.958 and 4.002 Å (in the complex), respectively (Table 6). Also, the bond angle of C7–N1–C8 is smaller in the complex (126.0°) compared to in the free ligand (130.1°) due to complex formation. The natural charges computed from the NBO analysis on the coordinated atoms are Pd (+0.715), O1 (−0.665), N1 (−0.483), O3 (−0.681) and O4 (−0.929) (Figure 8).

3.2.5 | Molecular DFT calculation of [Zn(OVAP)H_2O] complex

Figure 9 shows the optimized structures of the [Zn(OVAP)H_2O] complex as the lowest energy

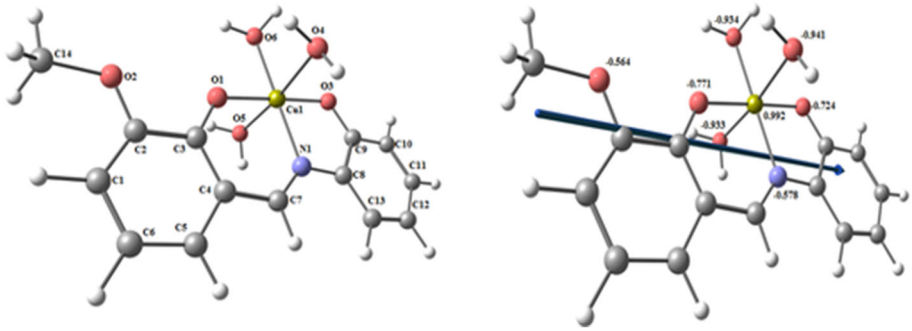

FIGURE 6 Optimized structure, vector of dipole moment, and natural charges on active centres of [Cu(OVAP)$(H_2O)_3$] using B3LYP/LANL2DZ. H atoms are omitted on C atoms for clarity

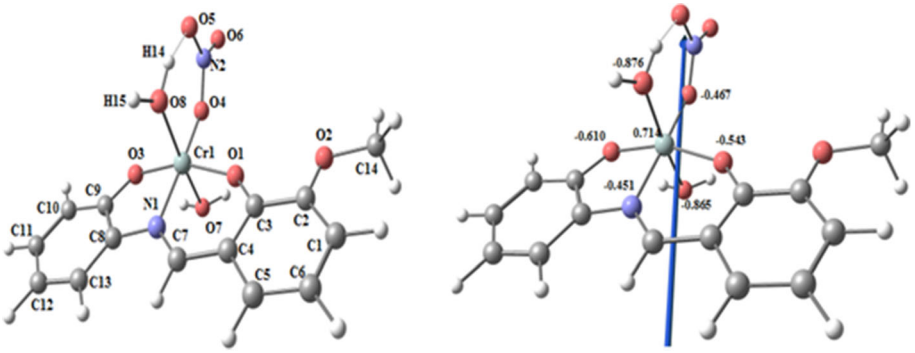

FIGURE 7 Optimized structure, vector of dipole moment, and natural charges on active centres of $[Cr(OVAP)NO_3(H_2O)_2]$ complex by density function B3LYP/LANL2DZ. H atoms are omitted on C atoms for clarity

TABLE 5 Important optimized bond lengths (Å) and bond angles (°) of OVAP and $[Cr(OVAP)NO_3(H_2O)_2]$ complex

Type of bond	Bond length(Å) Complex	Type of bond	Bond length(Å) OVAP	Complex
Cr–N1	2.052	O8–H14	—	1.027
Cr–O1	1.828	O8–H15	—	0.970
Cr–O3	1.886			
Cr–O4	2.043			
Cr–O7	2.122	O1···N1	4.024	2.713
Cr–O8	1.969	O1···O3	6.616	3.661
Type of angle	**Angle (°) Complex**	**Type of angle**	**Angle (°) Complex**	
N1–Cr–O1	88.56	O8–Cr–O1	99.17	
O1–Cr–O4	94.94	O8–Cr–O3	97.54	
N1–Cr–O3	81.88	O8–Cr–O4	92.22	
O3–Cr–O4	93.99	N1–Cr–O4	175.6	
O7–Cr–N1	98.72	O1–Cr–O3	160.7	
O7–Cr–O1	84.71	O7–Cr–O8	170.7	
O7–Cr–O3	80.26	N1–O7–O4–O8	0.378[a]	
O7–Cr–O4	78.96	O3–O8–O1–O7	−13.12[a]	
O8–Cr–N1	89.89	O1–N1–O3–O4	−9.251[a]	

[a]Dihedral angle.

configurations. The zinc atom is four-coordinate in geometry between distorted square planar and distorted tetrahedral configurations with atoms O1, N1, O3 and O4 deviating by 18.62° from the plane. The bond angles in the square planar geometry range from 78.16° to 106.7° (Table 7). The diagonal angle N1–Zn–O4 (154.2°) largely deviates from 180°, while O1–Zn–O3 (173.1°) is restricted by the tridentate ligand and is close to 180° (Table 7). The distances between donor atoms O1··· N1 and O1···O3 involved in coordination are largely decreased upon complex formation from 4.024 and 6.616 Å (in free ligand) to 2.958 and 4.002 Å (in the complex), respectively (Table 7). Also, the bond angle of C7–N1–C8 is smaller in the complex (126.4°) compared to in the free ligand (130.1°) due to complex formation. The natural charges computed from the NBO analysis on the coordinated atoms are Zn (+0.715), O1 (−0.665), N1 (−0.483), O3 (−0.681) and O4 (−0.929) (Figure 9).

Figure 10 shows the natural charges (obtained using NBO calculation) on the atoms of the ligand, which indicate large electron density (more negative) of the coordinated atoms N1, O1and O3. Figure 10 shows the molecular electrostatic potential surfaces, which describe the positive (blue colour) and the negative (red colour; bound loosely or excess electrons) charged electrostatic potential in the molecule. The computed total energy, the highest occupied molecular orbital (HOMO) energies, the lowest unoccupied molecular orbital (LUMO) energies and the dipole moment for the ligand and complexes were calculated (Figure 11 and Table 8). The more negative values of total energy of the complexes than those of free ligand indicate that the complexes are more stable than the free ligand. Also, the energy gaps ($E_g = E_{LUMO} - E_{HOMO}$) are smaller in the case of the complexes than in the ligand due to chelation of ligand to metal ions (Table 8). The lowering of E_g in complexes compared to ligand explains the charge transfer interactions upon complex formation.

3.3 | Complex–DNA binding

3.3.1 | Absorption titration analysis

The absorption titration technique is very useful, prominent and reliable for studying the binding mode of small

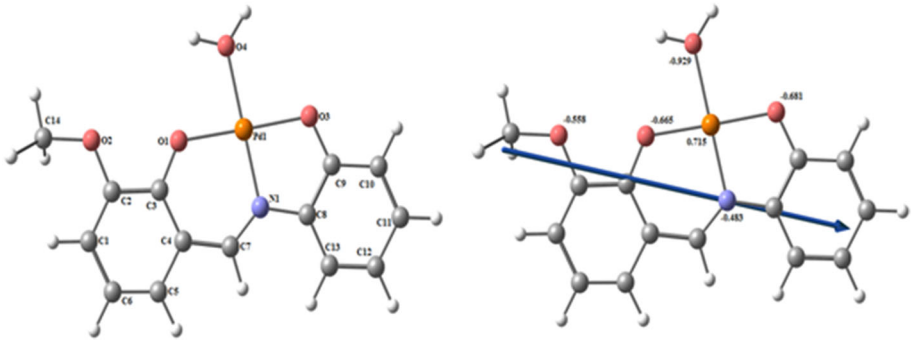

FIGURE 8 Optimized structure, vector of dipole moment, and natural charges on active centres of [Pd(OVAP)H_2O] complex by density function B3LYP/LANL2DZ. H atoms are omitted on C atoms for clarity

TABLE 6 Important optimized bond lengths (Å) and bond angles (°) of OVAP and [Pd(OVAP)H_2O] complex

Type of bond	Bond length(Å) Complex	Type of bond	Bond length(Å) OVAP	Complex
Pd–N1	1.971	Pd–O4	—	2.110
Pd–O1	1.991	O1···N1	4.024	2.958
Pd–O3	2.011	O1···O3	6.616	4.002
Type of Angle	**Angle (°) Complex**	**Type of Angle**	**Angle (°) Complex**	
N1–Pd–O1	96.56	N1–Pd–O3	179.9	
N1–Pd–O3	84.48	O1–Pd–O3	178.9	
O1–Pd–O4	83.50			
O3–Pd–O4	95.46	O1–N1–O3–O4	−0.380[a]	

[a]Dihedral angle.

molecules to a biopolymer like DNA. In this study, the binding mode of compounds to CT-DNA was investigated. Absorption spectra are very sensitive to changes in structure of compounds, and the structural change affects the absorption maxima. To determine the binding constant of the synthesized compounds to CT-DNA, we monitored the absorption maxima with gradual addition of DNA. For noncovalent interaction, i.e. intercalation, hypochromism with or without a red shift takes place;[6–9] while hyperchromism takes place for electrostatic binding. The observation of this study reflects the intercalative binding mode of the compounds to CT-DNA. Binding constants reflect the compound–DNA complex stability, while negative values of free energy indicate the spontaneity of compound–DNA binding.

The electronic absorption spectra of the metal complexes in the absence and presence of DNA are shown in Figure 12 and Figure S10. Table 9 presents spectral parameters for the interaction of DNA with the studied complexes. Upon gradual addition of DNA, the absorption intensities of ligand-to-metal charge transfer band gradually increased. As the DNA concentration is increased, a decrease of absorbance for each investigated complex was observed. Representative spectra illustrate this hypochromicity observed for the interaction of the investigated complexes with CT-DNA. With increasing amounts of DNA, the absorption bands of each investigated complex were affected. The determined intrinsic binding constants for the investigated complexes are in

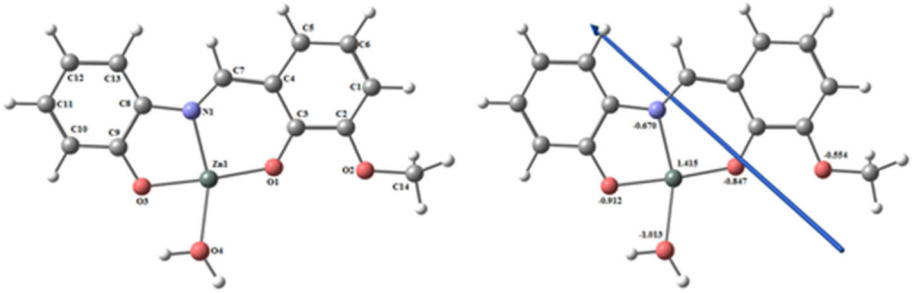

FIGURE 9 Optimized structure, vector of dipole moment, and natural charges on active centres of [Zn(OVAP)H_2O] complex by density function B3LYP/LANL2DZ. H atoms are omitted on C atoms for clarity

TABLE 7 Important optimized bond lengths (Å) and bond angles (°) of OVAP and [Zn(OVAP)H_2O] complex

Type of bond	Bond length(Å) Complex	Type of bond	Bond length(Å) OVAP	Complex
Zn–N1	2.068			
Zn–O1	1.914			
Zn–O3	1.981	O1···N1	4.024	2.898
Zn–O4	2.061	O1···O3	6.616	3.889
Type of angle	**Angle (°) Complex**	**Type of angle**	**Angle (°) Complex**	
N1–Zn–O1	93.33	N1–Zn–O4	154.2	
N1–Zn–O3	83.54	O1–Zn–O3	173.1	
O1–Zn–O4	106.7			
O3–Zn–O4	78.16	O1–N1–O3–O4	18.62[a]	

[a]Dihedral angle.

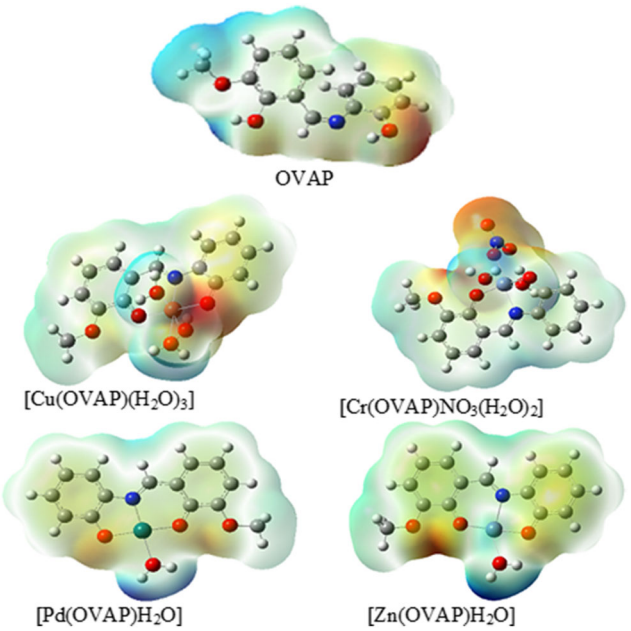

FIGURE 10 Molecular electrostatic potential surface of ligand (OVAP) and complexes ([Cu(OVAP)$(H_2O)_3$], [Cr(OVAP)$NO_3(H_2O)_2$], [Pd(OVAP)H_2O] and [Zn(OVAP)H_2O]) using B3LYP/LANL2DZ

the following order OVAPCr > OVAPZn > OVAPPd > OVAPCu. The free energy values of the prepared complexes are negative. This indicates the spontaneity of complex–DNA interaction.

3.3.2 | Hydrodynamic methods for investigation of DNA interaction with complexes

Optical spectroscopic tools provide significant, but not sufficient, evidence to support the binding mode for DNA interaction with the studied azomethine complexes. It is known that intercalation and groove binding affect the length of DNA, and hence the viscosity of DNA increases; while electrostatic binding does not affect the length of DNA and hence its viscosity remains constant.[29,32,58] Accordingly, to clarify the mode of interaction of the complexes with DNA, successive addition of complex to a fixed concentration of DNA was carried out. Upon addition of the prepared complexes, the relative viscosity of DNA increased as well as the respective complexes (Figure 13). This observation is explained on the basis that insertion of complex compound into the base pairs of DNA increases the length of the DNA chain and consequently increases the separation of base pairs which leads to the occurrence of intercalation of compounds into DNA.[29,32]

3.3.3 | Proposed mechanism of interaction with DNA

In our investigation, correlation between spectroscopic characteristics and hydrodynamic measurements of the interaction between the investigated complexes and DNA can suggest different binding modes. Most likely, DNA interacts through electrostatically or hydrophobically with the complexes. Since the OVAPCr complex gains positive charge as a result of replacement of nitrate ligand by H_2O molecules in solution,[29] an electrostatic interaction of the OVAPCr complex ion with negatively charged backbone in phosphate group at the periphery of the double helix of CT-DNA easily takes place. Also due to the removal of nitrate ligand from the complex in solution, the investigated complexes will have a flat part in the middle. Therefore, possible interaction of for example the OVAPCr complex with DNA could be as follows (Scheme 2):

- First, electrostatic interaction of coordination sphere with base pairs of DNA or interaction of Cr(III) complex with base backbone of DNA.
- Second, the flat part of the complex is inserted between the base pairs and consequently there is coordination of Cr^{3+} with base pairs of DNA.

For the OVAPPd complex, the possible interaction with DNA can occur through coordination of Pd(II) with

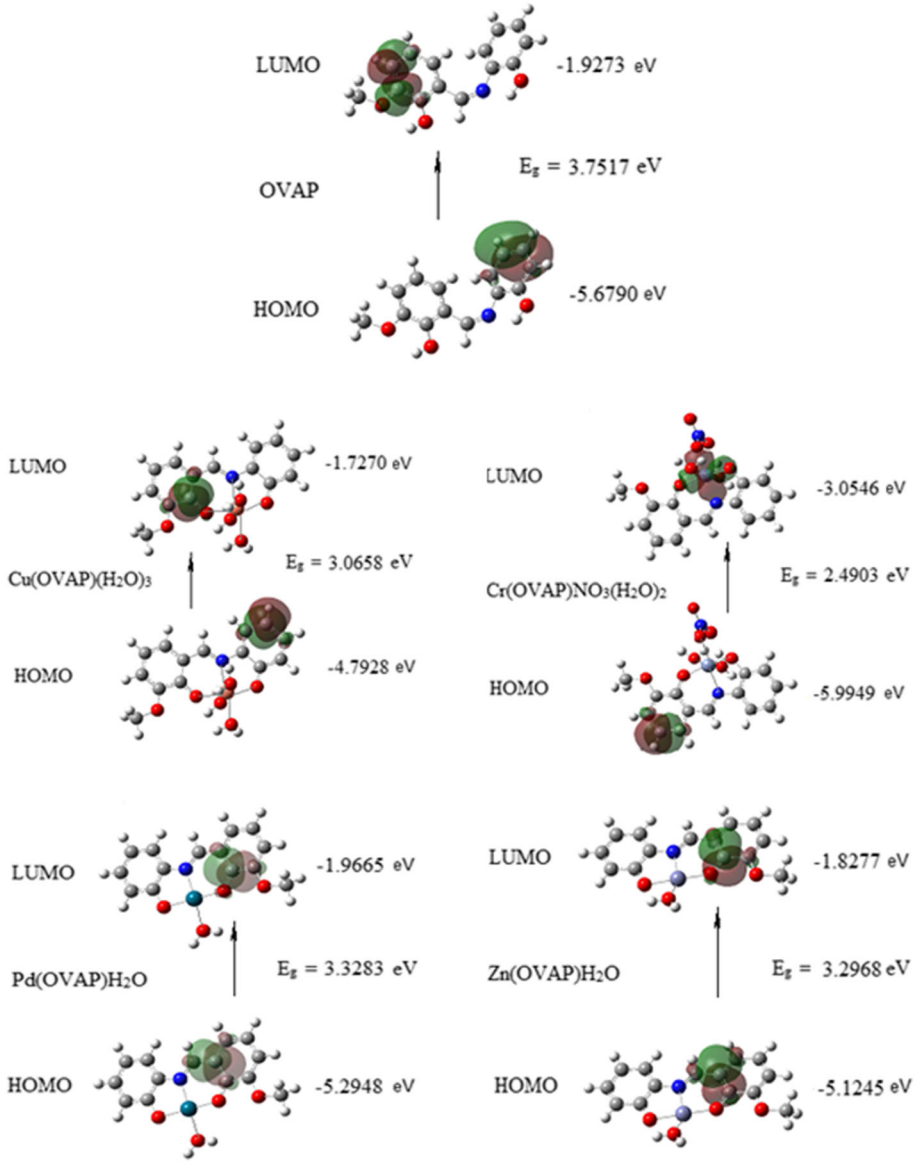

FIGURE 11 HOMO and LUMO charge density maps of ligand (OVAP) and complexes using B3LYP/LANL2DZ

TABLE 8 Calculated total energies, HOMO, LUMO, energy gap and dipole moments of OVAP azomethine ligand and its complexes at B3LYP/LANL2DZ level

	E^a	HOMO[b]	LUMO[c]	E_g[d]	Dipole moment (D)
OVAP	−821.590	−5.6790	−1.9273	3.7517	7.6786
$[Cu(OVAP)(H_2O)_3]$	−1245.897	−4.7928	−1.7270	3.0658	6.2332
$[Cr(OVAP)NO_3(H_2O)_2]$	−1432.862	−5.9949	−3.0546	2.4903	10.262
$[Pd(OVAP)H_2O]$	−1023.632	−5.2948	−1.9665	3.3283	3.6576
$[Zn(OVAP)H_2O]$	−962.521	−5.1245	−1.8277	3.2968	2.9618

[a]Total energy (a.u.).

[b]HOMO: highest occupied molecular orbital (eV).

[c]LUMO: lowest unoccupied molecular orbital (eV).

[d]Energy gap = $E_{LUMO} - E_{HOMO}$ (eV).

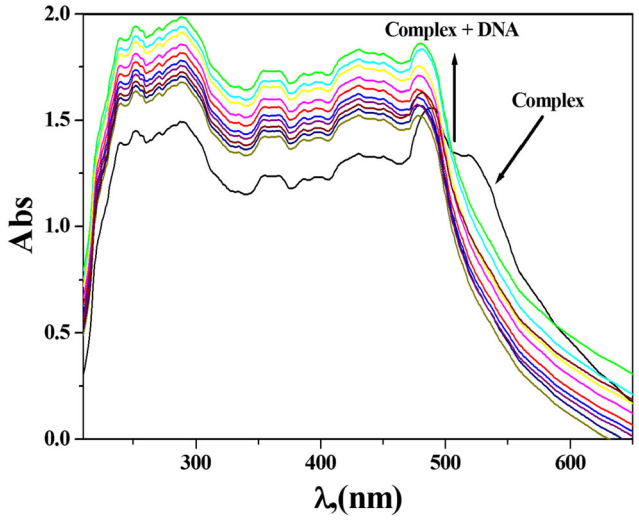

FIGURE 12 Absorption spectra of OVAPCr complex in 0.01 M Tris buffer (pH 7.5, 298 K) upon addition of CT-DNA in absence (lower) and presence of CT-DNA (top) at [OVAPCr] = 10^{-3} M and [CT-DNA] = 0–30 μM

base pairs of DNA through replacement binding mode and insertion of aromatic ring of OVAP ligand between base pairs of DNA (Scheme 3).

3.3.4 | DNA interaction via gel electrophoresis

The gel electrophoresis technique was used to investigate the binding of the investigated complexes with DNA. The results are shown in Figure 14. The technique involves comparing bands with different band widths and brightness to the control. The diversity in DNA cleavage efficiency of the investigated complexes was attributed to their difference in binding ability to DNA. It was clearly concluded that when complexes cleaved DNA, pathogenic growth was arrested through destruction of the genome of the organism.

TABLE 9 Spectral parameters for interaction of prepared azomethine complexes with DNA

Complex	λ_{max} free (nm)	λ_{max} bound (nm)	$n\Delta$	Chromism (%)[a]	Type of chromism	Binding constant ($\times 10^5$)[b]	ΔG (kJ mol^{-1})
OVAPPd	239	237	2	3.59	Hypo	2.38	−29.99
	318	317	1	31.75			
	429	410	19	41.25			
OVAPZn	240	239	1	5.29	Hypo	3.20	−30.71
	252	252	0	5.15			
	270	270	0	5.15			
	290	281	9	7.08			
	364	352	12	8.72			
OVAPCu	239	239	0	12.15	Hypo	1.30	−28.53
	252	252	0	11.76			
	271	270	1	11.83			
	289	289	0	11.52			
	361	362	−1	19.88			
	386	386	0	18.90			
	399	399	0	13.33			
	432	431	1	12.50			
OVAPCr	240	240	0	−12.23	Hyper	6.82	−32.54
	252	252	0	−12.41			
	270	270	0	−12.50			
	288	287	1	−12.08			
	361	361	0	−16.39			
	386	386	0	−14.75			
	398	398	0	−14.63			
	430	431	−1	−13.43			
	498	480	−19	2.56			

[a]Chromism (%) = $(Abs_{free} - Abs_{bound})/Abs_{free}$.

[b]Binding constant K_b in mol^{-1} dm^3.

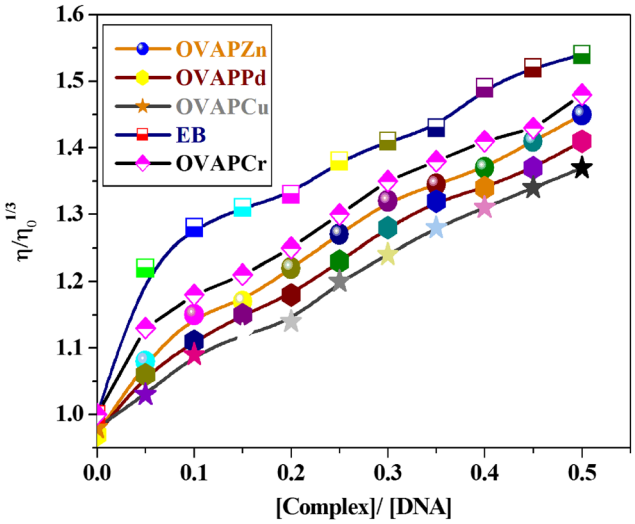

FIGURE 13 Effect of increasing amount of synthesized complexes on relative viscosities of CT-DNA at [DNA] = 0.5 mM at 298 K

3.4 | Antimicrobial activities

Many pathogens acquire resistance to antibiotics; therefore, a necessity for new antibiotics has arisen. Out of the five prepared compounds, the OVAPPd complex displayed broad-spectrum antimicrobial activity against all tested bacterial strains with MIC values of 4.25–6.00 μg l^{-1} (Tables 10 and 11; Figure 15). The investigated azomethine metal chelates reveal significantly enhanced antimicrobial activity against microbial strains in comparison to the free ligand (Tables 10 and 11; Figure 15). Hydrogen bond formation with azomethine group by the active sites is the proposed pathway of action of the metal chelates resulting in interference with cell wall synthesis. This hydrogen bond formation damages the cytoplasmic membrane and cell permeability may also occur resulting in the death of the cell. Certainly steric and pharmacokinetic factors also play a

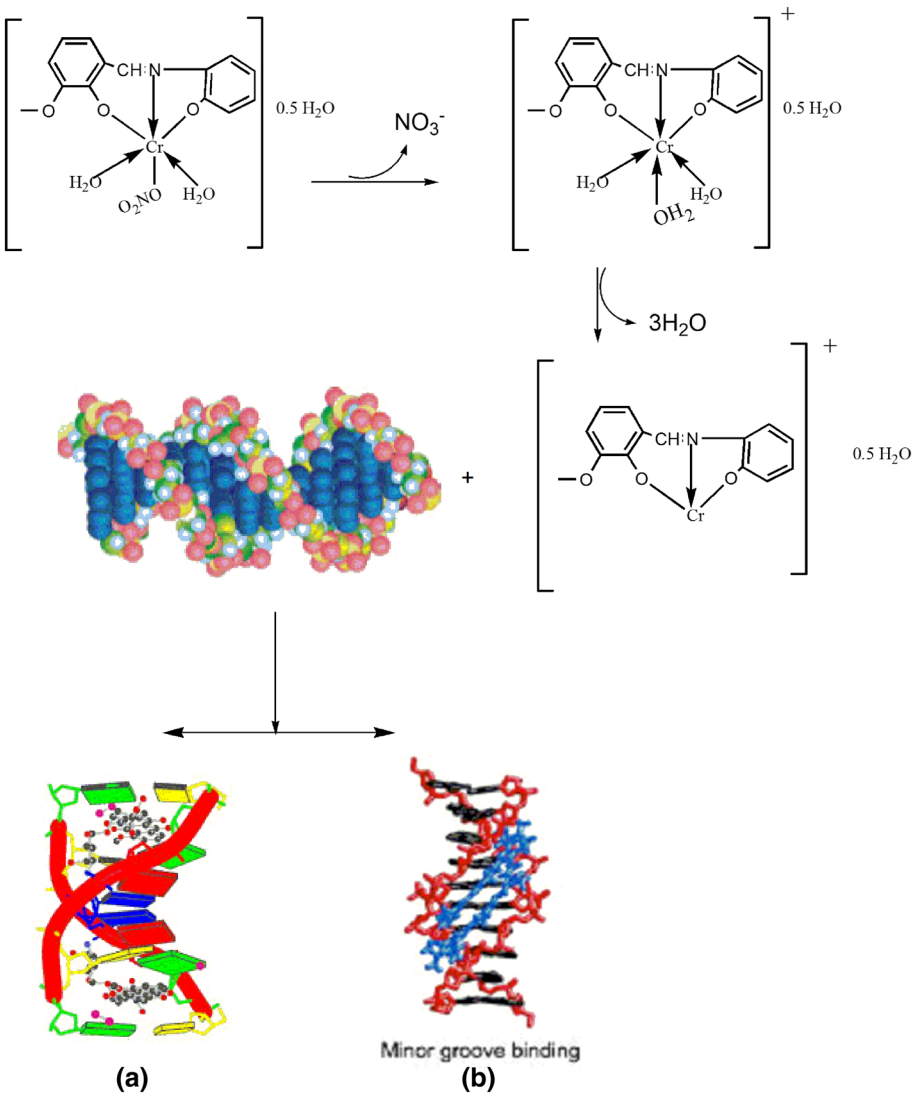

SCHEME 2 Suggested mechanism for interaction of OVAPPd with DNA via (a) intercalation binding mode

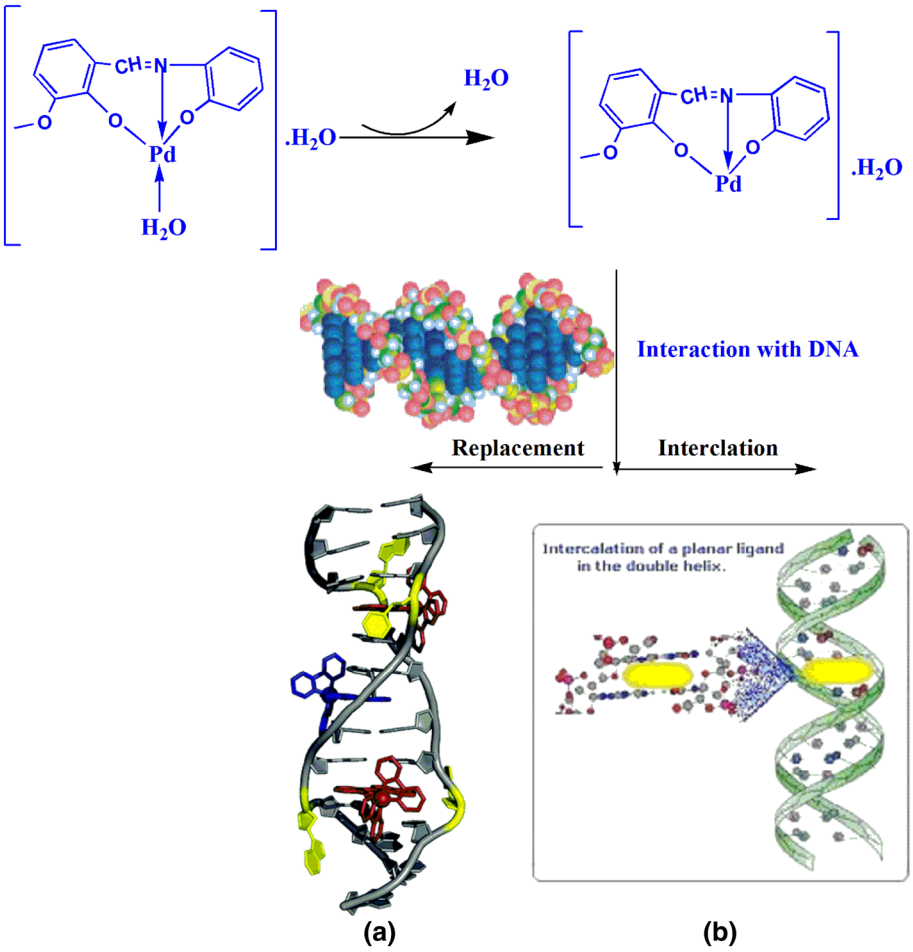

SCHEME 3 Suggested mechanism for interaction of OVAPPd with DNA via replacement binding mode

decisive role in deciding the potency of an antimicrobial agent. Thus, the antimicrobial property of metal complexes cannot be ascribed to chelation alone but it is an intricate blend of coordinating sites, nature of the metal ion, nature of the ligand, geometry of the metal chelate, and concentration, hydrophilicity, lipophilicity and the presence of co-ligands. The data reported in Table 10 show that the target azomethine OVAP ligand and its complexes are more efficient and active against Gram-positive than Gram-negative bacteria. This could be rationalized in terms of Gram-positive bacteria possessing a thick cell wall incorporating many layers of teichoic acids and peptidoglycan. On the other hand, Gram-negative bacteria possess a relatively thin cell wall of a few layers of peptidoglycan surrounded by a second lipid membrane incorporating lipoproteins and lipopolysaccharides. The variance in the structure of cell wall led to differences in antibacterial activity. The activities of the tested complexes were confirmed by calculating the potency index (Table S2) according to the following relation:[6–10]

$$\text{Activity index(A)} = \frac{\text{inhibition zone of complex(mm)}}{\text{inhibition zone of standard drug(mm)}} \times 100$$

On comparison of our obtained data with those of the literature, the activity of the palladium complex is higher than those of other complexes.[59,60] The determined properties of the synthesized compounds are of interest in terms of extending antibacterial and antifungal arsenal of existing drugs.

3.5 | Antioxidant activities

Free radical oxidative processes play a significant pathological role in causing many human diseases together with aging.[61] *In vitro* antioxidant activities of the newly synthesized OVAP azomethine ligand and its metal chelates were evaluated usingthe DPPH free radical scavenging method due to its ease and convenience. Sample solutions of different concentrations (10, 25,

FIGURE 14 Interaction of investigated complexes with CT-DNA studied by agarose gel electrophoresis. Lane 1: CT-DNA + OVAPPd; lane 2: CT-DNA + OVAPZn; lane 3: CT-DNA + OVAPCu; lane 4: CT-DNA + OVAPCr; lane 5: OVAPPd complex; lane 6: OVAPCu complex; lane 7: OVAPZn complex; lane 8: OVAPCr complex

50, 100 and 150 μg ml^{-1}) were prepared to evaluate the antioxidant activity. A solution of ascorbic acid was used as a standard for comparison. From the results obtained, it is clear that the metal chelates exhibit better antioxidant activity than the ligand. The results indicate that the antioxidant activity increases with increasing concentration for all complexes under study. In terms of IC50, the data show that the OVAPCu complex has potent antioxidant activity with the lowest IC50 value of 22 μg ml^{-1}, while the OVAPCr complex exhibited least antioxidant activity with IC50 of 75 μg ml^{-1}, as shown in Figure 16.

3.6 | Cytotoxicity studies

The anticancer activities of OVAP azomethine ligand and its metal chelates against HCT-116, HepG-2 and MCF-7 cells were screened using MTT assay. The results were analysed in terms of cell viability curves and expressed as IC_{50} values as shown in Figure 17 and Table S3. The

TABLE 10 Results of antimicrobial bioassay of prepared compounds against different strains of bacteria and fungi

Compounds	Inhibition zone ± SD (mm)											
	S. marcescence (−ve)		*E. coli* (−ve)		*M. luteus* (+ve)		*A. flavus*		*G. candidum*		*F. oxysporum*	
Conc. (μg ml^{-1})	15	30	15	30	15	30	15	30	15	30	15	30
OVAP	5.5 ± 0.10	8 ± 0.06	3.5 ± 0.11	6 ± 0.05	6.5 ± 0.07	10 ± 0.10	3 ± 0.14	6.5 ± 0.11	7.5 ± 0.05	13 ± 0.30	5.5 ± 0.21	8.5 ± 0.04
OVAPCr	13 ± 0.11	26.5 ± 0.10	10 ± 0.05	18.5 ± 0.13	17 ± 0.10	32 ± 0.23	9.5 ± 0.03	17.5 ± 0.31	18 ± 0.21	33.5 ± 0.12	11.5 ± 0.17	22 ± 0.14
OVAPPd	16.50 ± 0.05	33.5 ± 0.37	14 ± 0.20	25 ± 0.18	23 ± 0.11	41 ± 0.15	13.5 ± 0.14	23 ± 0.31	22.5 ± 0.31	39.5 ± 0.05	15 ± 0.13	27.50 ± 0.12
OVAPCu	14.50 ± 0.20	29.5 ± 0.17	12.5 ± 0.22	22 ± 0.11	21 ± 0.10	39 ± 0.16	12 ± 0.10	21.5 ± 0.31	22 ± 0.31	37.5 ± 0.17	14 ± 0.15	26 ± 0.13
OVAPZn	13.50 ± 0.10	27 ± 0.10	10.5 ± 0.05	19.50 ± 0.12	18 ± 0.05	35 ± 0.23	11 ± 0.05	19 ± 0.21	20 ± 0.25	35 ± 0.17	12 ± 0.17	23 ± 0.12
Ofloxacin	17 ± 0.11	35 ± 0.23	16 ± 0.15	27 ± 0.19	25 ± 0.18	43 ± 0.12						
Fluconazol							14.50 ± 0.21	24 ± 0.10	24 ± 0.04	41 ± 0.06	16.50 ± 0.21	29 ± 0.15

TABLE 11 Minimum inhibition zone for antimicrobial assay of prepared Schiff base and its complexes

	Bacteria			Fungi		
Compound	***M. luteus***	***E. coli***	***S. marcescence***	***A. flavus***	***G. candidum***	***F. oxysporum***
OVAP	10.00	10.70	9.00	10.75	9.00	9.50
OVAPCr	6.75	7.50	5.75	6.75	6.00	6.50
OVAPPd	4.25	6.00	4.75	5.00	4.50	4.75
OVAPCu	4.50	6.50	5.00	5.50	5.00	5.25
OVAPZn	5.50	7.25	5.50	6.25	5.25	5.75

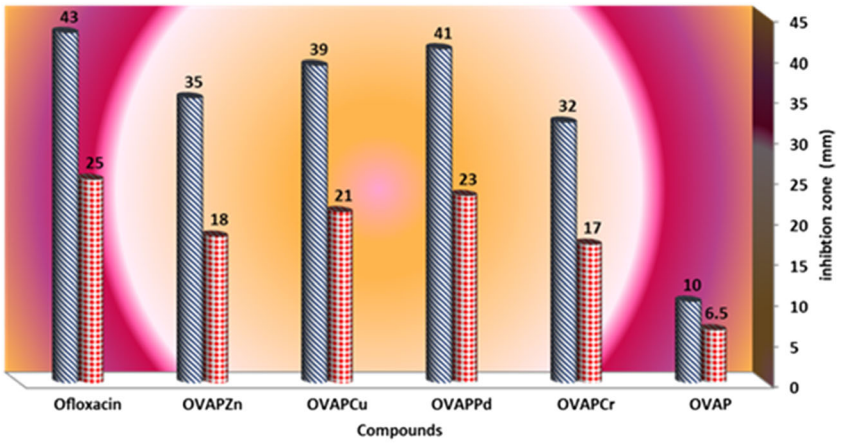

FIGURE 15 Histogram showing the comparative antibacterial activities of compounds against *M. luteus* (+ve) at 15 and 30 μg/ml

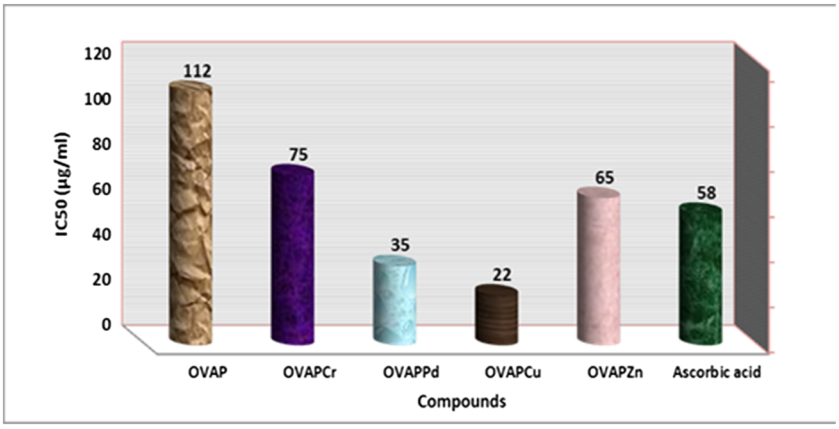

FIGURE 16 Trends in inhibition of DPPH radical by OVAP azomethine ligand and its complexes

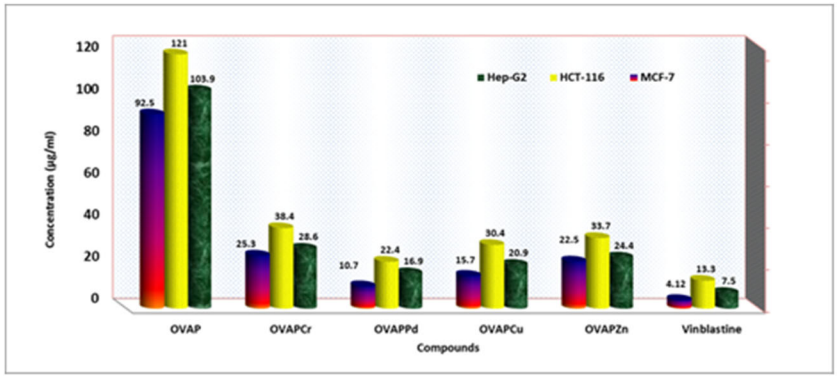

FIGURE 17 IC_{50} values of the ligand and its complexes against human colon carcinoma cells (HCT-116), hepatic cellular carcinoma cells (HepG-2) and breast carcinoma cells (MCF-7)

maximal inhibition concentrations (IC_{50}) given in Table S3 show that the cytotoxicity efficiencies of the compounds under investigation follow the order: OVAPPd > OVAPCu > OVAPZn > OVAPCr > OVAP ligand. From the results it is evident that the OVAPPd complex exhibited higher *in vitro* cytotoxicity against all selected cell lines when compared to the ligand as well as to the standard drug, vinblastine. In contrast, the OVAPCr complex showed lower anticancer activity when compared to the standard drug. It is generally thought that the cytotoxicity of metal chelates depends on their ability to bind DNA and thus damage its structure, which is followed by inhibition of replication and transcription processes and eventually cell death.[62,63] Thus, the higher cytotoxicity exhibited by the OVAPPd complex may be attributed to the stronger binding ability of that complex with DNA as discussed above. Cytotoxic agents can cause the death of a cell by several modes and among these necrosis and apoptosis are very prominent. Apoptosis or programmed cell death is characterized by blebbing of the plasma membrane, chromatin condensation and cell shrinkage.[64] On comparison of the cytotoxicity of the investigated compounds with results in the literature,[10,12] OVAPPd shows a potent activity against MCF-7 and HepG-2 cancer cell lines.

4 | CONCLUSIONS

The synthesis of four mononuclear complexes incorporating OVAP azomethine ligand derived from condensation of 2-hydroxy-3-methoxybenzaldehyde with 2-aminophenol and Pd(II), Zn(II), Cu(II) and Cr(III) has been described. The complexes were formed in 1:1 (ligand-to-metal) ratio as confirmed by microanalysis. The molar conductivity data of the complexes in DMF indicated that they are non-electrolytes. The structural features of the complexes were characterized from analytical and spectral data. Correlating between all characterization data and DFT calculations, the proposed structure of OVAPPd is square planar, OVAPZn is tetrahedral, OVAPCu is distorted octahedral whereas OVAPCr is octahedral. *In vitro* antimicrobial results show that the complexes have higher activities compared to the free ligand. The DNA binding studies suggest that the complexes bind to DNA mainly via intercalation. Cytotoxic activity of OVAPPd complex was higher against MCF-7 cell line than against the other investigated cancer cell lines compared to the other complexes. Furthermore, the prepared complexes show enhanced antioxidant activity compared with the OVAP azomethine ligand.

ORCID

Ahmed M. Abu-Dief https://orcid.org/0000-0003-3771-9011

REFERENCES

[1] N. K. Rasbi, H. Adams, I. Alshabibi, F. Al-Amri, *J. Photochem. Photobiol. A* **2014**, *285*, 37.

[2] R. Csonka, G. Speier, J. Kaizer, *RSC Adv.* **2015**, *5*, 18401.

[3] L. H. Abdel-Rahman, R. M. El-Khatib, L. A. E. Nassr, A. M. Abu- Dief, *J. Mol. Struct.* **2013**, *1040*, 9.

[4] L. H. Abdel-Rahman, R. M. El-Khatib, L. A. E. Nassr, A. M. Abu-Dief, M. Ismael, *Spectrochim. Acta A* **2014**, *117*, 366.

[5] A. M. Abu-Dief, L. A. E. Nassr, *J. Iran. Chem. Soc.* **2015**, *12*, 943.

[6] L. H. Abdel-Rahman, A. M. Abu-Dief, R. M. El-Khatib, S. M. Abdel-Fatah, *Bioorg. Chem.* **2016**, *69*, 140.

[7] L. H. Abdel-Rahman, A. M. Abu-Dief, M. O. Aboelez, A. A. H. Abdel-Mawgoud, *J. Photochem. Photobiol. B* **2017**, *170*, 271.

[8] L. H. Abdel-Rahman, A. M. Abu-Dief, M. Basha, A. A. Hassan Abdel-Mawgoud, *Appl. Organometal. Chem.* **2017**, *31*, e3750.

[9] L. H. Abdel-Rahman, A. M. Abu-Dief, R. M. El-Khatib, S. M. Abdel-Fatah, *Int. J. Nano. Chem.* **2018**, *4*, 1.

[10] L. H. Abdel-Rahman, A. M. Abu-Dief, M. R. Shehata, F. M. Atlam, A. A. H. Abdel-Mawgoud, *Appl. Organometal. Chem.* **2019**, *33*, e4699.

[11] M. Gaber, S. K. Fathalla, H. A. El-Ghamry, *Appl. Organometal. Chem.* **2019**, *33*, e4707.

[12] M. Gaber, N. El-Wakiel, K. El-Baradie, S. Hafez, *J. Iran. Chem. Soc.* **2019**, *16*, 169.

[13] L. H. Abdel-Rahman, R. M. El-Khatib, L. A. E. Nassr, A. M. Abu-Dief, F. E. D. Lashin, *Spectrochim. Acta A* **2013**, *111*, 266.

[14] A. M. Abu-Dief, M. A. Mohamed Ibrahim, *J. Basic Appl. Sci.* **2015**, *4*, 119.

[15] L. H. Abdel-Rahman, A. M. Abu-Dief, R. M. El-Khatib, S. M. Abdel-Fatah, *J. Photochem. Photobiol. B* **2016**, *162*, 298.

[16] L. H. Abdel-Rahman, A. M. Abu-Dief, M. Ismael, M. A. A. Mohamed, N. A. Hashem, *J. Mol. Struct.* **2016**, *1103*, 232.

[17] L. H. Abdel-Rahman, N. M. Ismail, M. Ismael, A. M. Abu-Dief, E. A. Ahmed, *J. Mol. Struct.* **2017**, *1134*, 851.

[18] L. H. Abdel-Rahman, A. M. Abu-Dief, N. M. Ismail, M. Ismael, *Inorg. Nano-Metal Chem.* **2017**, *47*, 467.

[19] L. H. Abdel-Rahman, R. M. El-Khatib, L. A. E. Nassr, A. M. Abu-Dief, *Arabian J. Chem.* **2017**, *10*, S1835.

[20] M. Gaber, A. M. Khedr, M. A. Mansour, M. Elsharkawy, *Appl. Organometal. Chem.* **2018**, *32*, e4606.

[21] M. Gaber, N. El-Wakie, O. M. Hemeda, *J. Mol. Struct.* **2019**, *1180*, 318.

[22] A. Vektariene, G. Vektaris, J. Svoboda, *ARKIVOC* **2009**, *7*, 311.

[23] H. M. Abd El-Lateef, A. M. Abu-Dief, A. A. Moniur, *J. Mol. Struct.* **2017**, *1130*, 522.

[24] H. M. Abd El-Lateef, A. M. Abu-Dief, B. El-Dien, M. El-Gendy, *J. Electroanal. Chem.* **2015**, *758*, 135.

[25] H. M. Abd El-Lateef, A. M. Abu-Dief, L. H. Abdel-Rahman, E. C. Sañudo, N. Aliaga-Alcalde, *J. Electroanal. Chem.* **2015**, *743*, 120.

[26] S. I. Al-Saeedi, L. H. Abdel-Rahman, A. M. Abu-Dief, S. M. Abdel-Fatah, T. M. Alotaibi, A. M. Alsalme, A. Nafady, *Catalysts* **2018**, *8*, 452.

[27] A. W. Coats, J. P. Redfern, *Nat. Sci.* **2012**, *4*, 170.

[28] E. M. M. Ibrahim, L. H. Abdel-Rahman, A. M. Abu-Dief, A. Elshafaie, S. K. Hamdan, A. M. Ahmed, *Phys. Scr.* **2018**, *93*, 055801.

[29] L. H. Abdel-Rahman, A. M. Abu-Dief, H. Moustafa, A. A. Hassan Abdel-Mawgoud, *Arabian J. Chem.* **2017**. https://doi.org/10.1016/j.arabjc.2017.07.007

[30] L. H. Abdel Rahman, A. M. Abu-Dief, N. A. Hashem, A. A. Seleem, *Int. J. Nano. Chem.* **2015**, *1*, 79.

[31] J. Marmur, *J. Mol. Biol.* **1961**, *3*, 208.

[32] L. H. Abdel-Rahman, A. M. Abu-Dief, E. F. Newair, S. K. Hamdan, *J. Photochem. Photobiol. B* **2016**, *160*, 18.

[33] L. H. Abdel-Rahman, A. M. Abu-Dief, A. A. H. Abdel-Mawgoud, *J. King. Saud Univ.* **2019**, *31*(1), 52.

[34] M. J. Pelczar, E. C. S. Chan, N. R. Krieg (Eds), Tata McGraw Hill Publishing, in *Tata McGraw Hill Publishing, in Microbiology*, 5th ed., New Delhi **1998**.

[35] P. Subbaraj, A. Ramu, N. Raman, J. Dharmaraja, *Int. J. Emerg. Sci. Technol.* **2013**, (1), 79.

[36] T. Mosmann, *J. Immunol. Methods* **1983**, *65*, 55.

[37] A. M. Abu-Dief, I. F. Nassar, W. H. Elsayed, *Appl. Organometal. Chem.* **2016**, *30*, 917.

[38] L. H. Abdel-Rahman, A. M. Abu-Dief, M. S. S. Adam, S. K. Hamdan, *Catal. Lett.* **2016**, *146*, 1373.

[39] L. H. Abdel Rahman, A. M. Abu-Dief, R. M. El-Khatib, S. M. Abdel-Fatah, A. M. Adam, E. M. M. Ibrahim, *Appl. Organometal. Chem.* **2018**, *32*, e4174.

[40] A. Elshafaie, L. H. Abdel-Rahman, A. M. Abu-Dief, S. Kamel Hamdan, A. M. Ahmed, E. M. M. Ibrahim, *NANO: Brief Rep. Rev.* **2018**, *13*, 1850074.

[41] L. H. Abdel-Rahman, A. M. Abu-Dief, A. A. H. Abdel-Mawgoud, *Int. J. Nano. Chem.* **2019**, *5*, 1.

[42] H. A. Bayoumi, A. M. A. Alaghaz, M. A. Aljahdali, *Int. J. Electrochem. Sci.* **2013**, *8*, 9399.

[43] L. H. Abdel-Rahman, A. M. Abu-Dief, S. K. Hamdan, A. A. Seleem, *Int. J. Nano. Chem.* **2015**, *1*, 65.

[44] M. Tyagi, S. Chandra, P. Tyagi, *Spectrochim. Acta A* **2014**, *117*, 1.

[45] D. Ray, P. K. Bharadwaj, *Inorg. Chem.* **2008**, *47*, 2252.

[46] A. A. A. Emara, *Spectrochim. Acta A* **2010**, *77*, 117.

[47] L. H. Abdel-Rahman, A. M. Abu-Dief, R. M. El-Khatib, S. M. Abdel-Fatah, A. A. Seleem, *Int. J. Nano. Chem.* **2016**, *2*, 82.

[48] M. Gaber, H. A. El-Ghamry, S. K. Fathalla, *Spectrochim. Acta A* **2015**, *139*, 396.

[49] M. Gaber, T. A. Fayed, M. M. El-Gamil, G. M. Abu El-Reash, *J. Mol. Struct.* **2018**, *1151*, 56.

[50] S. Perlepe, P. Jacobs, H. Desseyn, J. Tasangaris, *Spectrochim. Acta A* **1987**, *43*, 771.

[51] M. Gaber, H. El-Ghamry, F. Atlam, S. Fathalla, *Spectrochim. Acta A* **2015**, *137*, 919.

[52] T. A. Khan, S. S. Ghani, S. Naseem, *J. Coord. Chem.* **2010**, *63*, 4411.

[53] D. N. Kumar, B. S. Garg, *Spectrochim. Acta A* **2006**, *4*, 141.

[54] M. Gaber, H. A. El-Ghamry, S. K. Fathalla, M. A. Mansour, *Mater. Sci. Eng. C* **2018**, *83*, 78.

[55] C. R. Vinodkumar, M. K. Muraleedharan Nair, P. K. Radhakrishnan, *J. Therm. Anal. Calorim.* **2000**, *61*, 143.

[56] E. A. Abu-Gharib, R. M. EL-Khatib, L. A. E. Nassr, A. M. Abu-Dief, *Arabian J. Chem.* **2017**, *10*, S988.

[57] T. Hatakeyama, F. X. Quinn, *Thermal Analysis: Fundamentals and Applications to Polymer Science*, 2nd ed., John Wiley, Chichester **1994**.

[58] F. Arjmand, M. Aziz, *Eur. J. Med. Chem.* **2009**, *44*, 834.

[59] E. Pahontu, C. Paraschivescu, D. Ilies, D. Poirier, C. Oprean, V. Paunescu, A. Gulea, T. Rosu, O. Bratu, *Molecules* **2016**, *21*, 674.

[60] K. Sharma, M. K. Biyala, M. Swami, N. Fahmi, R. V. Singh, *Russ. J. Coord. Chem.* **2009**, *35*, 142.

[61] L. M. Gaetke, C. K. Chow, *Toxicology* **2003**, *189*, 147.

[62] S. Ramakrishnan, E. Suresh, A. Riyasdeen, M. A. Akbarsha, M. Palaniandavar, *Dalton Trans.* **2011**, *40*, 3245.

[63] L. H. Abdel-Rahman, M. S. Adam, A. M. Abu-Dief, H. Moustafa, M. Basha, A. H. Aboria, B. S. Al-Farhan, H. El-Sayed Ahmed, *Appl. Organometal. Chem.* **2018**, *32*, e4527.

[64] N. Tyagi, M. Viji, S. C. Karunakaran, S. Varughese, S. Ganesan, S. Priya, P. S. Saneesh Babu, A. S. Nair, D. Ramaiah, *Dalton Trans.* **2015**, *44*, 15591.

SUPPORTING INFORMATION

Additional supporting information may be found online in the Supporting Information section at the end of the article.

How to cite this article: Abu-Dief AM, El-Sagher HM, Shehata MR. Fabrication, spectroscopic characterization, calf thymus DNA binding investigation, antioxidant and anticancer activities of some antibiotic azomethine Cu(II), Pd(II), Zn(II) and Cr(III) complexes. *Appl Organometal Chem*. 2019;e4943. https://doi.org/10.1002/aoc.4943